Responses of the deep ocean carbonate system to carbon reorganization during the last glacial-interglacial cycle

Jimin Yu[1*], Robert F. Anderson[2], Zhangdong Jin[3], James W.B. Rae[4], Bradley N. Opdyke[1], Stephen M. Eggins[1]

[1]*Research School of Earth Sciences, The Australian National University, Canberra, ACT 0200, Australia*

[2]*Lamont-Doherty Earth Observatory of Columbia University, 61 Route 9W/PO box 1000, Palisades, NY, 10964-8000, USA.*

[3]*State Key Laboratory of Loess and Quaternary Geology, Institute of Earth Environment, Chinese Academy of Sciences, Xi'an 710075, China*

[4.] *Division of Geological and Planetary Sciences, California Institute of Technology, Pasadena, CA, 91125, USA*

*: Corresponding author: jimin.yu@anu.edu.au

Submit to *Quaternary Science Reviews* as an Article

Highlights:

- New $[CO_3^{2-}]$ for the intermediate Atlantic and deep Pacific during 0-160 ka;
- $[CO_3^{2-}]$ records show both temporal and transient changes that differ from $\delta^{13}C$;
- The MIS 5c-to-3 $[CO_3^{2-}]$ rise is consistent with the "coral-reef" hypothesis;
- Vertical carbon shifting affects $[CO_3^{2-}]$ variations at MIS 4 and 2;
- Deep water $[CO_3^{2-}]$ controlled $CaCO_3$ preservation in the deep Pacific.

Abstract

We present new deep water carbonate ion concentration ($[CO_3^{2-}]$) records, reconstructed using *Cibicidoides wuellerstorfi* B/Ca, for one core from Caribbean Basin (water depth = 3623 m, sill depth = 1.8 km) and three cores located at 2.3-4.3 km water depth from the equatorial Pacific Ocean during the last glacial-interglacial cycle. The pattern of deep water $[CO_3^{2-}]$ in the Caribbean Basin roughly mirrors that of atmospheric CO_2, reflecting a dominant influence from preformed $[CO_3^{2-}]$ in the North Atlantic Ocean. Compared to the amplitude of ~65 μmol/kg in the deep Caribbean Basin, deep water $[CO_3^{2-}]$ in the equatorial Pacific Ocean has varied by no more than ~15 μmol/kg due to effective buffering of $CaCO_3$ on deep-sea pH in the Pacific Ocean. Our results suggest little change in the global mean deep ocean $[CO_3^{2-}]$ between the Last Glacial Maximum (LGM) and the Late Holocene. The three records from the Pacific Ocean show long-term increases in $[CO_3^{2-}]$ by ~7 μmol/kg from Marine Isotope Stage (MIS) 5c to mid MIS 3, consistent with the response of the deep ocean carbonate system to a decline in neritic carbonate production associated with ~60 m drop in sea-level (the "coral-reef" hypothesis). Superimposed upon the long-term trend, deep water $[CO_3^{2-}]$ in the Pacific Ocean displays transient changes, which decouple with $\delta^{13}C$ in the same cores, at the start and end of MIS 4. These changes in $[CO_3^{2-}]$ and $\delta^{13}C$ are consistent with what would be expected from vertical nutrient fractionation and carbonate compensation. The observed ~4 μmol/kg $[CO_3^{2-}]$ decline in the two Pacific cores at >3.4 km water depth from MIS 3 to the LGM indicate further strengthening of deep ocean stratification, which contributed to the final step of atmospheric CO_2 drawdown during the last glaciation. The striking similarity between deep water $[CO_3^{2-}]$ and ^{230}Th-normalized $CaCO_3$ flux at two adjacent sites from the central equatorial Pacific Ocean provides convincing evidence that deep-sea carbonate dissolution dominantly controlled $CaCO_3$

preservation at these sites in the past. Our results offer new and quantitative constraints from deep ocean carbonate chemistry to understand roles of various mechanisms in atmospheric CO_2 changes over the last glacial-interglacial cycle.

Keywords: deep ocean carbonate ion, global carbon cycle, B/Ca, carbonate compensation, ocean stratification, Pleistocene

1. Introduction

Antarctic ice core records reveal that atmospheric CO_2 contents have varied systematically with Earth's climate during the past 800,000 years, displaying lower atmospheric CO_2 during cold glacials, by 80-100 ppm, than during warm interglacials (Lüthi et al., 2008). Proxy reconstructions and models suggest that the carbon stock of the land biosphere was ~500 GtC less during the Last Glacial Maximum (LGM, 19-23 ka) than during the Late Holocene (0-5 ka) (Bird et al., 1994; Ciais et al., 2012). Everything else being equal, introducing 500 GtC into the ocean-atmosphere system would elevate atmospheric CO_2 by ~45 ppm or, if deep ocean carbonate compensation is taken into account, by ~15 ppm (Sigman and Boyle, 2000). This leaves greater carbon storage in the ocean as the only viable reason for low atmospheric CO_2 during ice ages.

Changes in physical conditions of the ocean during the LGM have opposing influences on atmospheric CO_2: cooling of the ocean decreases atmospheric CO_2 by ~30 ppm, more saline seawater raises atmospheric CO_2 by ~6.5 ppm (Sigman and Boyle, 2000), and the reduction in

93 ocean volume raises atmospheric CO_2 by ~8 ppm (Brovkin et al., 2007). These changes lead to a
94 net decline in atmospheric CO_2 of ~15 ppm, which is barely enough to counter the atmospheric
95 CO_2 rise (~15 ppm) due to the contraction of terrestrial biosphere (Sigman and Boyle, 2000).
96 Therefore, explaining lower atmospheric CO_2 during ice ages clearly requires more complex
97 aspects of the ocean carbon cycle involving changes in ocean chemical composition, which is
98 greatly influenced by marine biological processes and oceanic carbonate burial/dissolution
99 budgets.
100
101 Nearly all hypotheses to decrease atmospheric CO_2 during glacials invoke greater
102 sequestration of carbon in the deep ocean (Broecker, 1982). However, evaluating the importance
103 of various processes that are thought to regulate atmospheric CO_2 on the timescales of
104 glacial/interglacial transitions has been challenging and controversial (Kohfeld et al., 2005;
105 Sigman and Boyle, 2000; Sigman et al., 2010). To fully understand reasons for atmospheric CO_2
106 changes in the past, it is necessary to accurately reconstruct the history of physiochemical
107 conditions of the ocean. Among many parameters, deep ocean carbonate ion concentration,
108 $[CO_3^{2-}]$, provides key information about the global carbon cycle in the past. To a first
109 approximation, $[CO_3^{2-}] \approx ALK - DIC$, where ALK is alkalinity and DIC is dissolved inorganic
110 carbon. Both ALK and DIC have profound influences on carbon storage in the ocean and hence
111 atmospheric CO_2. For example, the "nutrient deepening" hypothesis (Boyle, 1988a; Boyle,
112 1988b) suggests that a shift of carbon from the upper ocean to the deep ocean would increase
113 DIC while having a much smaller impact on ALK in deep waters. The resulting decrease in
114 $[CO_3^{2-}]$ would enhance $CaCO_3$ dissolution in the deep ocean. The enhanced deep-sea carbonate

115 dissolution disturbs the steady-state ALK input/output balance and leads to a net gain in the
116 oceanic ALK inventory, which lowers atmospheric CO_2.
117
118 Another mechanism to decrease atmospheric CO_2, which could occur during glaciations, is
119 the "coral reef" hypothesis (Berger, 1982; Opdyke and Walker, 1992). During marine
120 regressions, decreased coral growth, together with a general decline in neritic $CaCO_3$ burial due
121 to shrinking continental shelf availability, would drive up seawater ALK and [CO_3^{2-}], thus
122 lowering atmospheric CO_2 (Ridgwell et al., 2003a). Box models suggest that changes in oceanic
123 ALK associated with the ocean $CaCO_3$ preservation and production could account for up to 40
124 ppm variations in atmospheric CO_2 on glacial-interglacial timescales (Hain et al., 2010; Sigman
125 et al., 2010).
126
127 As illustrated by the examples above, deep ocean [CO_3^{2-}] is tightly linked to processes that
128 affect carbon reorganization in the ocean. Therefore, reconstructing the history of deep ocean
129 [CO_3^{2-}] will help constrain the roles of various processes in past atmospheric CO_2 changes
130 (Menviel et al., 2012). However, most published records are qualitative and often suffer
131 complicating factors such as pore water dissolution and surface productivity changes (Broecker,
132 2008). Quantitative deep ocean [CO_3^{2-}] reconstructions are only available at limited locations
133 (Marchitto et al., 2000; Marchitto et al., 2002; Raitzsch et al., 2011; Rickaby et al., 2010; Yu et
134 al., 2010a). At present, we have an insufficient number of quantitative [CO_3^{2-}] records to
135 constrain the roles of the "nutrient deepening" and "coral reef" hypotheses during the last
136 glaciation.
137

In this study, we present new deep water [CO_3^{2-}] records quantified using benthic B/Ca for four cores from the tropical Atlantic and Pacific Oceans over the last glacial-interglacial cycle. Combined with carbon isotopic ratios ($\delta^{13}C$) from the same cores, we investigate possible processes responsible for the transient and temporal [CO_3^{2-}] changes observed in our records and evaluate their roles in atmospheric CO_2 changes in the past. We also compare our deep water [CO_3^{2-}] with ^{230}Th-normalized $CaCO_3$ fluxes (Anderson et al., 2008) in two adjacent cores from the central deep equatorial Pacific Ocean to assess the roles of surface productivity (Marcantonio et al., 2001; Paytan et al., 1996) and deep-sea dissolution in controlling carbonate preservation at these sites during the last 160 ka.

2. Core materials and methods

We present paired benthic B/Ca and $\delta^{13}C$ for core VM28-122 at 3.6 km water depth (sill depth is 1.8 km) from the Caribbean Basin in the North Atlantic Ocean and three cores MW91-9 GGC15 (hereafter GGC15), MW91-9 GGC48 (hereafter GGC48) and TTNO13 PC61 (hereafter PC61) located respectively at 2.3 km, 3.4 km, and 4.3 km water depths from the equatorial Pacific Ocean (Table 1; Fig. 1). The age models for these cores are based on radiocarbon dates during the last ~30 ka and visual tuning of *Cibicidoides* $\delta^{18}O$ to the global benthic $\delta^{18}O$ stack (Lisiecki and Raymo, 2005) at older ages (Fig. 2). The age model of the deepest core PC61 is further supplemented by a slightly higher resolution *Pulleniatina obliquiloculata* $\delta^{18}O$ (Fig. 2D). During the last 160 ka, the sedimentation rates range from ~3-12 cm/ka at core VM28-122 to ~1-3 cm/ka at the three sites from the equatorial Pacific Ocean (Fig. 2). Despite their low sedimentation rates, benthic $\delta^{18}O$ of cores from the Pacific Ocean capture the expected structures shown by the global benthic $\delta^{18}O$ curve (Lisiecki and Raymo, 2005). One exception is the time

interval between Marine Isotope Stage (MIS) 6 and 5e at site GGC48, during which benthic $\delta^{18}O$ does not show an expected decrease during MIS 5e (from 130 to 122 ka) and the amplitude in $\delta^{18}O$ between MIS 5e and 6 is only ~1‰ compared to ~1.7‰ in the global benthic $\delta^{18}O$ curve (Fig. 2C). We suspect that data over MIS 6-5e in core GGC48 are likely compromised by bioturbation. Therefore, we refrain from discussing B/Ca data from 145-120 ka in this core.

We picked all benthic foraminifera including *C. wuellerstorfi* and other *Cibicidoides* genera from the >250 μm size fraction at sampling intervals of ~10 cm in core VM28-122, 2-4 cm in cores GGC15 and GGC48, and 1-2 (0-100 cm or 0-50 ka) to ~5 cm (100-270 cm) in core PC61. At site PC61, the high sampling rate for the 0-100 cm depth range is aimed to detect an expected $[CO_3^{2-}]$ spike at the last deglaciation. Picked *C. wuellerstorfi* were double checked under a microscope before crushing with due attention to use tests of most consistent morphology for B/Ca analyses throughout the cores (Rae et al., 2011). In general, the starting material for each B/Ca measurement has ~10 shells, equivalent to ~300 to 600 μg. When allowed by the shell availability, we carried out replicate B/Ca analyses. Foraminiferal shells were cleaned by the "Mg-cleaning" method (Barker et al., 2003) and different cleaning methods yielded similar B/Ca (Yu et al., 2007). Foraminiferal B/Ca were measured by ICP-MS using an established procedure (Yu et al., 2005). Because of the long residence time and the conservative nature of B in the ocean (Lemarchand et al., 2000), no significant change in [B] is expected on glacial-interglacial timescales. *C. wuellerstorfi* B/Ca were converted to deep-sea $[CO_3^{2-}]$ using a sensitivity of 1.14 μmol/mol per μmol/kg specific to this species obtained from a global core-top calibration (Fig. 3) by: $[CO_3^{2-}]_{downcore} = [CO_3^{2-}]_{preindustrial} + \Delta(B/Ca)/1.14$, where the preindustrial $[CO_3^{2-}]$ ($[CO_3^{2-}]_{preindustrial}$) is estimated using the GLODAP dataset (Key et al., 2004), and $\Delta(B/Ca)$ is the

184 deviation of B/Ca of down-core samples relative to the core-top value. Changes in temperature,
185 salinity, and water pressure (sea level) have a negligible effect on deep water [CO_3^{2-}] on glacial-
186 interglacial time scales (Yu et al., 2008). Existing data also suggest a minimal influence of
187 dissolution on benthic B/Ca (Yu et al., 2007; Yu and Elderfield, 2007). Based on replicate
188 analyses of a consistency standard and down-core samples, the average analytical uncertainty in
189 B/Ca is about ±3 μmol/mol (1 σ), corresponding to an error of ±2.5 μmol/kg in [CO_3^{2-}].
190
191 In most cases, we used *Cibicidoides* for $\delta^{18}O$ and $\delta^{13}C$ measurements to save *C. wuellerstorfi*
192 for B/Ca analyses. However, *C. wuellerstorfi* were the preferred species for $\delta^{18}O$ and $\delta^{13}C$
193 whenever they were available after B/Ca measurements. Foraminiferal $\delta^{18}O$ and $\delta^{13}C$ were
194 measured at University of Cambridge with the average analytical error of ~0.08‰ in both $\delta^{18}O$
195 and $\delta^{13}C$. Bulk sediment carbonate content (%$CaCO_3$) data for core PC61 were provided by W.
196 S. Broecker at LDEO of Columbia University, with an analytical precision of ~ ±1%.
197
198 Some of the data presented here have been published previously. Benthic $\delta^{18}O$ and $\delta^{13}C$ over
199 the last ~30 ka in VM28-122 are from (Oppo and Fairbanks, 1990) and all *C. wuellerstorfi* B/Ca
200 from this core have been published for proxy evaluation purposes (Yu et al., 2010b).
201 Radiocarbon dates, benthic B/Ca, and $\delta^{18}O$ and $\delta^{13}C$ over the last ~30 ka for cores VM28-122,
202 GGC15 and GGC48 are from (Yu et al., 2010a). In total, new measurements presented here
203 include 354 paired $\delta^{18}O$ and $\delta^{13}C$, 271 B/Ca, 6 radiocarbon dates, and 76 %$CaCO_3$, which are
204 tabulated in the Supplementary Materials. Wherever applicable, we note data sources in figure
205 captions.
206

3. Results

3.1. Core-top calibration

Although our major focus here are down-core records, we take this opportunity to present new core-top B/Ca that expands the geographic coverage of the original calibration (Fig. 3). All core-tops are judged to be the Late Holocene (<5 ka) in age. Deep water carbonate saturation state with respect to calcite, $\Delta[CO_3^{2-}]$, overlying these core-tops are estimated using the GLODAP dataset (Key et al., 2004), following the approach described in Yu and Elderfield (2007).

Fig. 3 shows core-top B/Ca in the benthic foraminifera *C. wuellerstorfi* and *C. mundulus* against deep water $\Delta[CO_3^{2-}]$ from five studies (Brown and Elderfield, 1996; Rae et al., 2011; Raitzsch et al., 2011; Yu and Elderfield, 2007; this study). Altogether, we have 212 and 68 B/Ca measurements (including replicates) at 152 and 48 core-top sites for *C. wuellerstorfi* and *C. mundulus*, respectively. B/Ca ratios were analyzed by two techniques including solution ICP-MS and laser ablation ICP-MS in four laboratories. Core-top B/Ca and deep water $\Delta[CO_3^{2-}]$ are tightly correlated with high R^2 values of 0.81-0.83 (Fig. 3). Regressions on B/Ca (including replicates) yield sensitivities of B/Ca versus deep water $\Delta[CO_3^{2-}]$ of 1.14 and 0.69 μmol/mol per μmol/kg for *C. wuellerstorfi* and *C. mundulus*, respectively, which are indistinguishable from those originally published in (Yu and Elderfield, 2007). Using the averaged B/Ca of replicates for regression analyses would have negligible influences on intercepts and slopes (see Fig. 3 caption). Due to the scatter in our calibration (see below), we have applied linear regression analyses to the data in Fig. 3, although eight *C. wuellerstorfi* samples from deep water $\Delta[CO_3^{2-}]$ < -15 μmol/kg plot below the calibration line. More core-tops from low deep water $\Delta[CO_3^{2-}]$ are

needed to investigate whether there is any change in the B/Ca-$\Delta[CO_3^{2-}]$ sensitivity. The compilation in Fig. 3 strengthens the calibration in Yu and Elderfield (2007).

Despite the strong correlation, an individual data point may deviate from the regression line by up to ~15 μmol/mol (Fig. 3). The scatter may come from the following sources: (i) inter-shell B/Ca variability of up to ~10 μmol/mol, which may be due to bioturbation mixing of shells of different ages, as revealed by duplicate analyses of core-top samples (~8 shells per sample) (Yu and Elderfield, 2007); (ii) intra-shell B/Ca variability of up to ~100 μmol/mol (or ±43%) probably introduced by biological influences ("vital effects") (Raitzsch et al., 2011); (iii) B/Ca variability up to ~40 μmol/mol associated with different morphologies within the same species ("vital effects") (Rae et al., 2011); and (iv) uncertainties associated with deep water $\Delta[CO_3^{2-}]$ estimates (~±5-10 μmol/kg) for core-top shells calcified over the last ~5 ka. It is possible that the integrated uncertainties in B/Ca may be largely determined by factor (i), but further work is needed to evaluate B/Ca variabilities at sites of different sedimentation rates. Large variability in ratios has also been observed in other proxies such as benthic Mg/Ca (±51%; compared to ±43% in B/Ca) (Raitzsch et al., 2011), Cd/Ca (Boyle, 1984, 1995), and $\delta^{18}O$ (McCave et al., 2005; Sortor and Lund, 2011), and we know these proxies offer valuable information about paleoceanography. Indeed, core-top B/Ca ratios from different studies plot along the same trend (Fig. 3) and the down-core B/Ca record from the Caribbean Sea, which was published before acknowledging "noise" from (ii) and (iii), shows a pattern that is consistent with $\delta^{11}B$ over the last 160 ka (Yu et al., 2010b).

252 Various sources of noise mentioned above highlight the need to practice caution when
253 interpreting relatively small [CO_3^{2-}] changes down core. To improve the signal to noise ratio, we
254 suggest the following practical approaches: (i) use high sedimentation rate cores to minimize the
255 effect of bioturbation, just as one would do when working on other proxies; (ii) use multiple
256 shells, ideally as many as possible and preferably >8 shells per analysis in practice, to obtain
257 integrated B/Ca ratios that are minimally influenced by intra-shell variability; (iii) use shells of
258 the most consistent morphology throughout the core; and (iv) make replicate measurements,
259 when possible, to evaluate overall uncertainty.
260
261 **3.2. Down-core B/Ca results**
262 During the last 160 ka, *C. wuellerstorfi* B/Ca in core VM28-122 from the North Atlantic
263 varied between ~185 and 260 μmol/mol, corresponding to a range of ~65 μmol/kg in deep water
264 [CO_3^{2-}] (Fig. 4A). Due to the shallow sill depth of Caribbean Basin (~1800 m), core VM28-122
265 records intermediate water chemistry in the past (Ribbat et al., 1976) (Fig. 1). By comparison, the
266 amplitudes in B/Ca in the three cores from the western and central equatorial Pacific Ocean are
267 much smaller, exhibiting ~165-180 μmol/mol in GGC15, ~145-165 μmol/mol in GGC48 and
268 ~130-155 μmol/mol in PC61, respectively (Fig. 4B-D). These variations in B/Ca suggest a
269 maximum change of ~15 μmol/kg in deep water [CO_3^{2-}] at the three sites from the equatorial
270 Pacific Ocean during the last full glacial-interglacial cycle.
271
272 Down-core *C. wuellerstorfi* B/Ca at VM28-122 mimics that of $\delta^{11}B$ in *Globigerinoides ruber*
273 from the tropical Atlantic (Foster, 2008; Henehan et al., 2013), showing high deep water [CO_3^{2-}]
274 during cold periods (MIS 2, 4, 6) and low values during relatively warm periods (MIS 1, 3, 5)

(Fig. 4A). Results for the three cores from the equatorial Pacific Ocean show different patterns between themselves and differ significantly from those at site VM28-122. B/Ca-derived deep water [CO_3^{2-}] at the shallowest site (GGC15; 2.3 km water depth) in the western equatorial Pacific Ocean display similar values during the last 50 ka and at late MIS 6, interrupted by low values during MIS 5 and early MIS 4 (Fig. 4B). At 3.4 km water depth, B/Ca ratios in core GGC48 suggest a [CO_3^{2-}] spike at the last deglaciation, similar deep water [CO_3^{2-}] values during MIS 3 and at the core-top, and significantly decreased [CO_3^{2-}] at MIS 2, 4, and 5b-d (Fig. 4C). At site PC61 from 4.3 km water depth in the central equatorial Pacific Ocean, a spike in deep water [CO_3^{2-}] is also discernable at the last deglaciation (Fig. 4D), but is less obvious than at core WIND 28 (10.2^{o}S, 51.8^{o}E, 4147 m) from the deep Indian Ocean (Yu et al., 2010a), possibly due to lower sedimentation rates at PC61. At site PC61, we observe high deep water [CO_3^{2-}] at MIS 3 and 6 and low values at MIS 2, 4, and 5d-e. Table 2 summarizes deep water [CO_3^{2-}] for a few time intervals and [CO_3^{2-}] differences between them at four studied sites.

Despite their differences in detail, all three records from the equatorial Pacific Ocean show long-term rises in deep water [CO_3^{2-}] from MIS 5c to mid-MIS 3 and transient decreases(increase) in [CO_3^{2-}] at the onset(end) of MIS 4 (Fig. 4B-D; Table 2).

4. Discussion

4.1. Deep ocean [CO_3^{2-}] between the Late Holocene and LGM and implications

The elevated deep water [CO_3^{2-}] at core VM28-122 during the LGM fits well with previous reconstructions (Yu et al., 2008) (Fig. 5) and is consistent with substantial ocean circulation changes in the North Atlantic Ocean (Lippod et al., 2012; Lund et al., 2011; Marchitto et al.,

298 2002; Oppo and Lehman, 1993; Yu et al., 2008). In line with foraminiferal assemblage and
299 benthic Zn/Ca results (Anderson and Archer, 2002; Marchitto et al., 2005), reconstructions on
300 the three cores from the equatorial Pacific Ocean and one core (WIND 28K) from the
301 southwestern Indian Ocean (Yu et al., 2010a) reveal much smaller changes of -5 to 3 μmol/kg
302 between the LGM and the Late Holocene (Fig. 5; Table 2). These small changes point to
303 efficient buffering of deep-sea $CaCO_3$ on deep water pH in the Indo-Pacific Oceans (Anderson
304 and Archer, 2002). During the LGM, the global deep ocean [CO_3^{2-}] at >~3.5 km water depth
305 appeared to be more homogeneous relative to the late Holocene, because [CO_3^{2-}] decreased in
306 the deep North Atlantic and slightly increased in the deep Indo-Pacific Oceans (Fig. 5),
307 consistent with previous modeling work (Emerson and Archer, 1992).
308
309 Although large in amplitude, changes in deep water [CO_3^{2-}] in the Atlantic Ocean may have
310 relatively modest impacts on the global mean deep ocean [CO_3^{2-}] because (i) the Atlantic is
311 relatively small in volume (~25% of the global ocean) and (ii) opposite changes in [CO_3^{2-}] at
312 shallow and deep water depths tend to cancel their influences on the global mean deep ocean
313 [CO_3^{2-}] (Fig. 5). It is expected that changes in deep water [CO_3^{2-}] in the Indian and Pacific
314 Oceans, where the largest volume of the global seawater is stored, should impose the dominant
315 influence on the global mean deep water [CO_3^{2-}]. Supported by foraminiferal assemblage
316 estimates (Anderson and Archer, 2002), the small variations in deep water [CO_3^{2-}] for cores
317 located at 2.3-4.3 km water depth in the Indian and Pacific Oceans (this study; Yu et al., 2010a)
318 suggest that the global mean deep ocean [CO_3^{2-}] is likely similar between the LGM and the Late
319 Holocene.
320

Similar global mean deep water [CO_3^{2-}] between the LGM and the Late Holocene places important constraints on factors influencing the global carbon cycle and low atmospheric CO_2 during glacials. First, little change in the global mean deep water [CO_3^{2-}] strengthens the previous view that transportation of $\delta^{13}C$-depleted terrestrial carbon to the ocean (Curry et al., 1988), as opposed to a carbonate ion effect on the carbon isotope incorporation into benthic tests (Lea et al., 1999), caused the ~0.32‰ decrease in benthic $\delta^{13}C$ during the LGM. Second, neither the "rain ratio" nor "silica leakage" hypothesis can be a primary mechanism for low atmospheric CO_2 during glacials because both hypotheses would require a significant increase in the deep ocean [CO_3^{2-}] during the LGM (Kohfeld et al., 2005), which is not supported by our reconstructions. Third, since carbon lost from the atmosphere and the land biosphere must have been stored as DIC in the deep ocean during glacials (Broecker, 1982), little change in the global mean deep ocean [CO_3^{2-}] suggests that deep ocean ALK (≈ [CO_3^{2-}] + DIC) during the LGM must have been higher than today, consistent with previous model results (Toggweiler, 2008). By increasing CO_2 solubility in seawater, high ocean ALK helps to lower atmospheric CO_2 during glacials (Hain et al., 2010; Sigman et al., 2010).

Our results are obviously at odds with the ~100 μmol/kg higher [CO_3^{2-}] in the glacial deep ocean based on $\delta^{11}B$ measurements on mixed benthic foraminifera (Sanyal et al., 1995). $\delta^{11}B$ from Sanyal et al. (1995) are likely compromised by "vital effects" (Hönisch et al., 2008; Rae et al., 2011) and/or analytical uncertainties (Foster et al., 2006). Our estimate is also in contrast to a previous reconstruction in the Weddell Sea, which suggests that glacial deep water [CO_3^{2-}] was ~25 μmol/kg higher than during interglacials (Rickaby et al., 2010; Zeebe and Marchitto, 2010). However, the sedimentation rate of the Weddell Sea core is low with only 3 data points during

344 the last 20 ka, warranting further work in the Southern Ocean to investigate deep water carbonate
345 chemistry in this region (Zeebe and Marchitto, 2010).
346
347 **4.2. Deglacial deep ocean [CO_3^{2-}] spikes**
348 Modeling work suggests that the release of carbon from the deep ocean and associated
349 carbonate compensation would produce [CO_3^{2-}] peaks in the Indian and Pacific Oceans during
350 deglaciations (Boyle, 1988a; Boyle, 1988b; Broecker and Peng, 1987). We see no deglacial
351 [CO_3^{2-}] peak at cores VM28-122 and GGC15, maybe due to circulation changes as discussed
352 previously (Yu et al., 2010a). During the LGM, VM28-122 and GGC15 would be affected by
353 intermediate waters formed in the North Atlantic and North Pacific, respectively (Boyle and
354 Keigwin, 1987; Matsumoto et al., 2002). With dense sampling in the top 100 cm (1 sample every
355 1-2 cm), our B/Ca ratios at site PC61 indeed resolve a [CO_3^{2-}] peak during the last deglaciation
356 (Fig. 6G). This peak is centered at ~9 ka, slightly later than the timing (~14-10 ka) observed at a
357 shallower core GGC48 from the Pacific Ocean (Fig. 6E) and at core WIND 28K from the deep
358 Indian Ocean (Yu et al., 2010a) (Supplementary Fig. S1). This age offset is probably an artifact
359 of strong bioturbation due to low sedimentation rates at site PC61 (Fig. 2D), highlighting the
360 need for high-resolution in the Pacific Ocean. The decline in deep water [CO_3^{2-}] during the
361 Holocene at site PC61 is about 10 μmol/kg, comparable to a previous estimate of 10-15 μmol/kg
362 based on a dissolution model (Berelson et al., 1997). The evolution of deep water [CO_3^{2-}] at site
363 PC61 during the last deglaciation is consistent with deep ocean carbon release and carbonate
364 compensation discussed previously (Yu et al., 2010a). We therefore refer reader to (Yu et al.,
365 2010a) for the interpretation of the last deglacial [CO_3^{2-}] records from the equatorial Pacific
366 Ocean.

Changes in deep Pacific [CO_3^{2-}] at the penultimate deglaciation are less comprehensive, because we only have two records at sites GGC15 and PC61 extending back to MIS 6 (Fig. 6C, G). Deep water [CO_3^{2-}] at 4.3 km water depth core PC61 appears to show a simple decline of ~7 μmol/kg from MIS 6 to 5e, instead of a deglacial spike (Table 2). Our record at 2.3 km water depth core GGC15 is too short to reveal an unambiguous spike at the penultimate deglaciation. At this site, the obvious decline in [CO_3^{2-}] of ~7 μmol/kg from MIS 6 to 5 is in stark contrast to stable [CO_3^{2-}] during the last ~30 ka. These observations suggest that deep ocean [CO_3^{2-}] must have responded differently during the last two glacial terminations. This conclusion is consistent with %$CaCO_3$ at ODP 1089 from Cape Basin, a qualitative record of deep water [CO_3^{2-}] (Hodell et al., 2001), which shows a broad peak at ~190-120 ka (the penultimate deglacial) compared to a narrow %$CaCO_3$ spike at the last deglaciation. More records, especially for the penultimate deglaciation, are needed to investigate reasons for different variations in deep water [CO_3^{2-}] between the two terminations.

4.3. Deep Pacific [CO_3^{2-}] rise from MIS 5c to 3 and sea-level drop

Details aside, all three cores from the Pacific Ocean show long-term increases in deep water [CO_3^{2-}], by ~7 μmol/kg, from MIS 5c to mid MIS 3 (Fig. 6C, E, G; Table 2). Because these cores cover a large water depth range (2.3-4.3 km) in the equatorial Pacific Ocean which hosts the largest volume of the global seawater, the observed increases probably reflect a response of the global mean deep ocean [CO_3^{2-}]. The much greater amplitude change at core VM28-122 in the Caribbean Basin over the same time interval (Fig. 6A; Table 2) is likely due to large changes in the pre-formed [CO_3^{2-}] in the North Atlantic Ocean (Foster, 2008; Yu et al., 2010b). In the North

390 Atlantic, surface seawater [CO_3^{2-}] during the LGM was about 60 μmol/kg greater than the Late
391 Holocene (Yu et al., 2013).
392
393 During the last glaciation, deceasing temperatures, vegetation and precipitation would reduce
394 the global chemical erosion rate on continents (Broecker and Peng, 1987). However, exposure of
395 carbonates on the shelves, which weather at a faster rate than other rock types, tends to increase
396 the global chemical erosion rate (Gibbs and Kump, 1994). Therefore, the alkalinity flux from
397 rivers to the ocean may have remained roughly constant in the past, and may not be responsible
398 for the long-term rise in deep ocean [CO_3^{2-}]. Pelagic carbonate production in the past is poorly
399 constrained, with some studies suggest higher export production during the LGM than during
400 MIS 5a-d (e.g., Kohfeld et al., 2005; Menviel et al., 2012; Paytan et al., 1996), which would
401 decrease the deep ocean [CO_3^{2-}] from MIS 5c to 3, opposite to the trend observed in our records.
402
403 We argue that the long-term rise in [CO_3^{2-}] in the Pacific Ocean from MIS 5c to mid MIS 3 is
404 consistent with the "coral reef" hypothesis (Berger, 1982; Opdyke and Walker, 1992) (Fig. 7A).
405 This rise in deep Pacific [CO_3^{2-}] coincided with a global sea-level drop of ~60 m (Fig. 6I) (Grant
406 et al., 2012; Thompson and Goldstein, 2006; Waelbroeck et al., 2002). Today, shallow water
407 carbonate production makes up about half of the global $CaCO_3$ burial (Opdyke and Walker,
408 1992) and a drop of 60 m in sea-level would result in a substantial loss of the shelf area and
409 hence a decrease in neritic carbonate production and preservation (Milliman, 1974, 1993).
410 Everything else being equal, a decrease in carbonate deposition on shelves would raise the global
411 ALK and DIC at a ratio of 2:1, resulting in an increase in the whole ocean [CO_3^{2-}] (≈ ALK –
412 DIC) which deepens the calcite saturation horizon and improves $CaCO_3$ preservation in the deep

413 sea. By raising deep ocean [CO_3^{2-}], a sea-level drop shifts the locus of carbonate deposition from
414 the shelves to the deep sea, helping to maintain the whole ocean ALK balance (Berger, 1982;
415 Menviel and Joos, 2012; Opdyke and Walker, 1992; Ridgwell et al., 2003b). The associated gain
416 in oceanic ALK due to the decline in coral growth during marine regression contributes to the
417 decrease in atmospheric CO_2 (Fig. 6J). Our results provide important constraints for models to
418 quantify the role of the "coral reef" hypothesis in atmospheric CO_2 declines during the last
419 glaciation.
420

421 **4.4. Transient [CO_3^{2-}] changes at MIS 4 and carbonate compensation**

422 Superimposed upon the long-term rise (Section 4.3), deep water [CO_3^{2-}] records at all three
423 sites from the equatorial Pacific Ocean show transient changes at MIS 4 (Fig. 6C, E, G). These
424 changes differ from variations in benthic $\delta^{13}C$ from the same cores (Fig. 6D, F, H). For example,
425 at the start of MIS 4, deep water [CO_3^{2-}] at site GGC15 declined by ~7 μmol/kg and coincided
426 with a ~0.3‰ decrease in benthic $\delta^{13}C$ (Fig. 6C, D). While $\delta^{13}C$ stayed low for ~10,000 years
427 during MIS 4, [CO_3^{2-}] recovered back to the long-term trend within ~7,000 years. At the end of
428 MIS 4, the opposite changes occurred. Similar patterns in [CO_3^{2-}] and $\delta^{13}C$ are also observed at
429 sites GGC48 and PC61 (Fig. 6E-H), although amplitudes slightly differ. The reoccurrence of
430 similar patterns in [CO_3^{2-}] and $\delta^{13}C$ from all three cores lead us to believe that these changes are
431 robust features of the deep ocean carbonate system at MIS 4 in the Pacific Ocean. Furthermore,
432 we rely on the relative variations in [CO_3^{2-}] and $\delta^{13}C$ from the same cores to minimize any
433 complications from age model uncertainties.
434

435 The observed changes in [CO_3^{2-}] and $\delta^{13}C$ at MIS 4 cannot be explained by changes in the
436 pre-formed values in the North Atlantic, because records at site VM28-122 show general
437 increases in both [CO_3^{2-}] and $\delta^{13}C$ during MIS 4 (Fig. 6A, B). At the onset of MIS 4, sea-level is
438 thought to have dropped by ~50 m (Fig. 6I) (Grant et al., 2012; Thompson and Goldstein, 2006;
439 Waelbroeck et al., 2002) and any decrease in neritic carbonate production associated with the
440 sea-level drop should have driven up ocean [CO_3^{2-}] (Section 4.3), opposite to the observed
441 decreases in [CO_3^{2-}] at the three sites from the Pacific Ocean (Fig. 6C, E, G). Instead, we argue
442 that the observed changes in [CO_3^{2-}] and $\delta^{13}C$ at MIS 4 are consistent with vertical nutrient
443 fractionation (i..e, a shift of nutrient and presumably carbon between shallow and deep water
444 depths) and carbonate compensation (Fig. 7B) (Boyle, 1988a; Boyle, 1988b; Broecker and Peng,
445 1987).
446
447 During the transition from MIS 5 to 4, marine sediment evidence indicates the first
448 significant increases in dust fluxes, surface nutrient utilization, and marine export production in
449 the Subantarctic zone of the Southern Ocean (Francois et al., 1997; Hain et al., 2013; Kohfeld et
450 al., 2005; Kumar et al., 1995; Lambert et al., 2008; Martinez-Garcia et al., 2011; Robinson and
451 Sigman, 2008). At this transition, benthic $\delta^{13}C$ increased by ~0.4‰ in the upper North Atlantic
452 Ocean (Fig. 6B) and decreased by ~0.5-1.5‰ at greater water depths (>~3 km) in the global
453 ocean (Fig. 8) (Hodell et al., 2003; McCave et al., 2005; Mix, 2001; Ruddiman et al., 1989).
454 These observations agree well with the nutrient deepening hypothesis that invokes sequestration
455 of biological carbon from the surface and upper oceans to the deep ocean at the start of MIS 4
456 (Boyle, 1988a; Boyle, 1988b).
457

458 By shifting the aqueous carbonate equilibrium $CO_2 + CO_3^{2-} + H_2O \leftrightarrow 2HCO_3^-$ to the right,
459 sequestration of carbon in the deep ocean would initially lower deep-sea $[CO_3^{2-}]$, as observed in
460 our records from the Pacific Ocean (Fig. 6C, E, G), and enhance $CaCO_3$ dissolution in the deep
461 ocean at the onset of MIS 4 (Crowley, 1983; Hodell et al., 2001; Le and Shackleton, 1992;
462 Raitzsch et al., 2011). Assuming constant pelagic $CaCO_3$ production and weathering rate,
463 increased $CaCO_3$ dissolution in the deep ocean caused by accumulation of respiratory CO_2,
464 together with a decline in neritic $CaCO_3$ production due to the sea-level drop (Section 4.3),
465 would elevate ocean ALK and DIC at a ratio of 2:1, leading to a rise in seawater $[CO_3^{2-}]$ until a
466 balance between ALK input from rivers and deep-sea $CaCO_3$ burial is reestablished on a
467 timescale of ~7,000 years (Fig. 7B) (Archer et al., 2000; Broecker and Peng, 1987). Carbonate
468 compensation has little effect on seawater $\delta^{13}C$ and would decouple $[CO_3^{2-}]$-$\delta^{13}C$ during the
469 recovery stage of the deep ocean carbonate system, which is observed in our records (Fig. 6C-H;
470 Fig. 7B). At the end of MIS 4, the opposite changes in $[CO_3^{2-}]$ and $\delta^{13}C$ are in line with "nutrient
471 shoaling" (Boyle, 1988a; Boyle, 1988b). As discussed previously, both initial carbon
472 reorganization and the associated carbonate compensation affect atmospheric CO_2 (Archer et al.,
473 2000; Broecker and Peng, 1987; Hain et al., 2010; Menviel et al., 2012). Our results provide
474 critical constraints for models to quantify their respective roles in atmospheric CO_2 changes at
475 MIS 4.
476
477 **4.5. Changes in $[CO_3^{2-}]$ from MIS 3 to the LGM**
478 Deep water $[CO_3^{2-}]$ records show contrasting trends from MIS 3 to the LGM. In the
479 Caribbean Basin, deep water $[CO_3^{2-}]$ rose by ~ 7 μmol/kg (Fig. 6A), likely reflecting an increase
480 in pre-formed $[CO_3^{2-}]$ in response to a decrease in atmospheric CO_2 (Lüthi et al., 2008) (Fig. 6J),

481 due to its proximity to the deep water formation sites in the North Atlantic Ocean (Fig. 1). In the
482 Pacific Ocean, we observe little change in deep water [CO_3^{2-}] at site GGC15 and ~4 μmol/kg
483 decrease at sites GGC48 and PC61 from mid MIS 3 to the LGM (Fig. 6C, E, G; Table 2).
484 Although generally weaker than in the Atlantic, circulation changes in the Pacific Ocean might
485 be significant enough to overwhelm deep ocean [CO_3^{2-}] at sites close to water mass boundaries.
486 Benthic $\delta^{13}C$ results suggest an existence of new water mass above ~2 km water depth in the
487 North and Equatorial Pacific, whereas the North Pacific Deep Water deepened from today's 1-2
488 km to >3 km water depth during the LGM (Herguera et al., 2010; Keigwin, 1998; Leduc et al.,
489 2010; Matsumoto et al., 2002; McCave et al., 2008) (Fig. 1). A change in the structure of water
490 masses in the Pacific Ocean could cause different evolutions of deep water [CO_3^{2-}] at the three
491 sites from the Pacific Ocean from the MIS 3 to the LGM (Fig. 6C, E, G).
492
493 Located at 4.3 km water depth in the central Pacific Ocean, site PC61 may have been
494 minimally affected by ocean circulation changes, so the ~4 μmol/kg decrease in [CO_3^{2-}] between
495 MIS 3 and the LGM recorded at this site is interpreted to reflect the change in deep Pacific
496 carbonate chemistry independent of changes in ocean circulation. Reconstructions using benthic
497 B/Ca showed a decline of ~5 μmol/kg over the same time interval in the deep (>~4 km water
498 depth) North and Equatorial Atlantic and Indian Oceans (Raitzsch et al., 2011; Yu et al., 2010a).
499 Dissolution indices also indicated deteriorated carbonate preservation from MIS 3 to the LGM in
500 the deep Atlantic, Indian, and Pacific Oceans (Barker et al., 2006; Bickert and Mackensen, 2003;
501 Crowley, 1983; Farrell and Prell, 1989, 1991; Hodell et al., 2001; Howard and Prell, 1994; Le
502 and Shackleton, 1992). Therefore, it seems that the MIS 3-to-LGM decrease in deep water
503 [CO_3^{2-}] is widespread in the global deep ocean (>~4 km water depth).

504

505 As shown by previous model results (Opdyke and Walker, 1992), a sea level drop of ~30 m
506 from the mid MIS 3 to the LGM (Grant et al., 2012; Thompson and Goldstein, 2006;
507 Waelbroeck et al., 2002) (Fig. 6I) would increase in the global mean deep ocean [CO_3^{2-}],
508 opposite to our observation (Fig. 7A, Section 4.3). Although an increase in pelagic $CaCO_3$
509 production would lead to a decrease in deep ocean [CO_3^{2-}], we dismiss this possibility for three
510 reasons. First, while permanently decreasing deep ocean [CO_3^{2-}], an increase in pelagic $CaCO_3$
511 production would deepen the Carbonate Compensation Depth (CCD) during the first few
512 thousand years of the surface production increase and result in a decoupling of deep ocean
513 carbonate saturation horizon and CCD (Sigman and Boyle, 2000), evidence for which is lacking.
514 Second, the steady increase in [CO_3^{2-}] from MIS 5c to mid MIS 3 (Fig. 6C, E, G) must require
515 that any increase in the surface $CaCO_3$ production rate should not exceed the rate of decline in
516 neritic $CaCO_3$ production until mid MIS 3, a strict condition to satisfy. Third, an increase in
517 surface $CaCO_3$ productivity would increase atmospheric CO_2, opposite to the observed decline
518 from ice cores (Lüthi et al., 2008) (Fig. 6J). Currently, paleo-proxy data are inconclusive on
519 changes in the pelagic rain rate of $CaCO_3$ in the past (Menviel et al., 2012).
520

521 We argue that an increased in ocean stratification is responsible for the widespread decreases
522 in deep water [CO_3^{2-}] observed at our sites GGC48 and PC61 as well as at other locations in the
523 Atlantic and Indian Oceans (Raitzsch et al., 2011; Yu et al., 2010a). From MIS 3 to the LGM the
524 deep ocean (>~3 km) may have become further stratified (Adkins et al., 2002; Burke and
525 Robinson, 2012; Lund et al., 2011) and sequestered more respired carbon, as suggested by
526 decreases in benthic $\delta^{13}C$ over this time interval (Fig. 6F, H; 8). During the LGM, stratification

and the efficiency of the biological pump might have reached its maximum potential (Hain et al., 2013), overwhelming the increase in deep ocean [CO_3^{2-}] due to lowering sea level (Section 4.3). Increased sequestration of respired carbon is further supported by low deep water O_2 deduced from increased authigenic uranium in sediments (Bradtmiller et al., 2010; Jaccard et al., 2009). The associated shift of carbon to greater depths would transiently decrease [CO_3^{2-}] in the deep ocean (Boyle, 1988a; Boyle, 1988b), explaining the observed decreases at site PC61 and other locations. Carbonate compensation should bring the deep ocean [CO_3^{2-}] back to a steady state within ~7,000 years (Archer et al., 2000; Boyle, 1988a; Boyle, 1988b; Broecker and Peng, 1987), seemingly inconsistent with the sustained low [CO_3^{2-}] for ~10,000 years during MIS 2 at site GGC48 (Fig. 6E). However, we note that, in addition to the influence from the global deep ocean stratification, site GGC48 may be further affected by deepening of NPDW during the LGM (Matsumoto et al., 2002). The expected recovery of deep water [CO_3^{2-}] due to $CaCO_3$ compensation during the LGM at core PC61 is not evident in our data (Fig. 6G), which may be caused by strong bioturbation at low sedimentation rates (Fig. 2D). More importantly, any rise in deep water [CO_3^{2-}] in response to deep ocean carbonate compensation during MIS 2 might have been overwhelmed by carbon release due to a change in deep ocean vertical stratification during the last deglaciation (Anderson et al., 2009). We suggest that increased vertical ocean stratification at the transition of MIS 3 to the LGM has contributed to the 20 ppmv decrease in atmospheric CO_2 at the final step of the last glaciation (Lüthi et al., 2008) (Fig. 6J) by sequestering carbon in the deep ocean and by increasing ocean ALK through deep ocean $CaCO_3$ dissolution.

4.6. Inter-ocean [CO_3^{2-}] gradient and atmospheric CO_2

550 Fig. 9 shows the differences in $[CO_3^{2-}]$ and $\delta^{13}C$ between sites VM28-122 and PC61, in
551 comparison with atmospheric CO_2 during the last 160 ka. Differencing $[CO_3^{2-}]$ and $\delta^{13}C$ between
552 the two sites removes influences from "open-system" responses including deep ocean carbonate
553 compensation, changes in neritic carbonate production associated with sea-level fluctuations, and
554 transportation of terrestrial biosphere carbon to the ocean, all of which should be global and
555 impose equal impacts on chemical properties at different locations. These open-system processes
556 sometimes can significantly affect changes in deep water $[CO_3^{2-}]$ and $\delta^{13}C$ at a given location
557 caused by processes within the ocean interior. In contrast, gradients in $[CO_3^{2-}]$ and $\delta^{13}C$ between
558 cores VM28-122 and PC61 should mainly reflect "closed-system" processes such as ocean
559 circulation, ocean stratification, and biological respiration that redistribute DIC and ALK among
560 different volumes of the ocean. Over the last 160 ka, both $[CO_3^{2-}]$ and $\delta^{13}C$ gradients co-vary
561 with atmospheric CO_2, showing large gradients during MIS 2, 4, and 6 when atmospheric CO_2
562 was low (Fig. 9A, B). Furthermore, $[CO_3^{2-}]$ and $\delta^{13}C$ gradients are positively correlated and plot
563 along the Redfield slope (Yu et al., 2008) (Fig. 9C). Deep water $[CO_3^{2-}]$ and $\delta^{13}C$ at VM28-122
564 are negatively correlated with atmospheric CO_2 over the last 160 ka, but they plot along a
565 shallower slope than the Redfield ratio on the $\delta^{13}C$-$[CO_3^{2-}]$ space (Supplementary Fig. S2).
566 Differencing $[CO_3^{2-}]$ and $\delta^{13}C$ between sites VM28-122 and PC 61 slightly improves the
567 correlation and, importantly, increases the $\delta^{13}C$-$[CO_3^{2-}]$ slope close to the Redfield ratio (Fig. 9).
568
569 The results in Fig. 9 are consistent with the "ocean stratification" hypothesis (Francois et al.,
570 1997; Sigman and Boyle, 2000). Deep water $[CO_3^{2-}]$ and $\delta^{13}C$ at core VM28-122 suggests that
571 this site has been bathed by a water mass located above the stratification boundary (Yu et al.,
572 2010b). Located in the abyss of the Pacific Ocean, core PC 61 likely records the maximum

impact of nutrient deepening associated with the deep ocean stratification. Stratification and associated nutrient accumulation in the deep ocean would drive both [CO_3^{2-}] and $\delta^{13}C$ in opposite directions for cores VM28-122 and PC61, leading to greater [CO_3^{2-}] and $\delta^{13}C$ gradients between the two sites when stratification was strengthened. Therefore, greater gradients in [CO_3^{2-}] and $\delta^{13}C$ together with decreases in atmospheric CO_2 during MIS 2, 4, and 6 (Fig. 9) suggest stepwise strengthening of deep ocean stratification has played an important role in atmospheric CO_2 drawdown during the last glaciation.

The recent "ventilation volume" hypothesis (Kwon et al., 2012) suggests that a large volume of glacial deep ocean was ventilated by deep waters formed in the North Atlantic which is characterized by low pre-formed nutrient and high $\delta^{13}C$. According to this idea, any increase in seawater nutrient in the ocean's interior would mainly reflect a greater regeneration of biogenic carbon and hence a stronger biological pump which acts to lower atmospheric CO_2 (Hain et al., 2013; Kwon et al., 2012). In this case, and excluding influences from carbonate compensation, changes in deep water [CO_3^{2-}] and $\delta^{13}C$ should be correlated and plot along the Redfield slope (Yu et al., 2008), which is observed in Fig. 9C. Therefore, our data appear to be consistent with the "ventilation volume" hypothesis as a feasible mechanism for changes in atmospheric CO_2 in the past (Hain et al., 2013; Kwon et al., 2012).

4.7. $CaCO_3$ preservation in the central deep Equatorial Pacific Ocean

Since its discovery by Arrhenius (1952), the origin of the "Pacific-type" %$CaCO_3$ pattern remains debated, centering on whether surface productivity or deep-sea dissolution controls downcore variability of $CaCO_3$ accumulation (Anderson et al., 2008; Archer, 1991; Hodell et al.,

596 2001; Lyle et al., 2000; Lyle et al., 1992). Fig. 10 shows a comparison of B/Ca derived deep
597 water [CO_3^{2-}], %$CaCO_3$, and ^{230}Th-normalized $CaCO_3$ flux for two adjacent cores from the
598 central Pacific Ocean (Anderson et al., 2008). Considering the data over the entire studied time
599 interval, deep water [CO_3^{2-}] and ^{230}Th-normalized $CaCO_3$ flux show striking similarities during
600 the last 160 ka. Therefore, along with little change in surface productivity based on ^{230}Th-
601 normalized Ba and ^{10}Be (Anderson et al., 2008; Marcantonio et al., 2001; Paytan et al., 1996),
602 our data provide convincing evidence for deep ocean dissolution as a dominant control on $CaCO_3$
603 accumulation in the central deep Pacific Ocean during the last glacial-interglacial cycle
604 (Anderson et al., 2008; Berelson et al., 1997).
605
606 We also observe some differences in our records. During MIS 5, %$CaCO_3$ at site PC61 is
607 higher than that at PC72 (Fig. 10A), possibly suggesting different degrees of sediment focusing
608 even at closely located cores, or possibly reflecting the southward decrease in dust (lithogenic)
609 accumulation across the equatorial Pacific (see Fig. 4 of (Anderson et al., 2006)), which would
610 have had the greatest impact on measured %$CaCO_3$ during periods of minimal $CaCO_3$
611 preservation, such as MIS 5. Deep water [CO_3^{2-}] differs from the ^{230}Th-normalized $CaCO_3$ flux
612 mainly during MIS 5 and 2. During MIS 5, [CO_3^{2-}] at site PC61 exhibited large fluctuations with
613 three short-term excursions, in contrast to stable ^{230}Th-normalized $CaCO_3$ fluxes at site PC72.
614 The difference may be due to the selective preservation of a small number of whole foraminifera
615 shells used for B/Ca. Although the periods of elevated [CO_3^{2-}] were brief, compared to
616 background periods of lower [CO_3^{2-}], the benthic foraminifera that lived during periods of high
617 [CO_3^{2-}] were preferentially preserved, thereby biasing the population of specimens that survived
618 in favor of periods of high [CO_3^{2-}]. By contrast, Th-normalization integrates fragments from

619 periods of poor preservation (most of the time) with whole foraminiferal shells (preferentially
620 preserved, but representing only a small portion of the integrated time interval). Because of the
621 nature of these different measurements, it is necessary to have a longer period of high [CO_3^{2-}] to
622 detect the effect in Th-normalized $CaCO_3$ flux in cores with low accumulation rates.
623 Alternatively, the difference may be caused by a lower sampling resolution in core PC72 (12
624 samples in PC61 versus 6 samples in PC72 during 72-128 ka). During MIS 2, the [CO_3^{2-}] minima
625 seems to occur ~3,000 years later than the minima in ^{230}Th-normalized $CaCO_3$ flux (Fig. 10B),
626 which could be an artifact of bioturbation for low sedimentation rates (~2 cm/ka) at both sites
627 (Fig. 2D).
628
629 **5. Conclusions**
630 Based on paired [CO_3^{2-}] and $\delta^{13}C$ records from Caribbean Basin and the equatorial Pacific
631 Ocean, we reach the following conclusions:
632
633 (1) Over the last glacial-interglacial cycle, deep water [CO_3^{2-}] at the mid-depth of the North
634 Atlantic Ocean displays a large amplitude variability of ~65 μmol/kg, reflecting strong
635 influences from surface ocean chemistry in this well ventilated water mass. In contrast, deep
636 water [CO_3^{2-}] at three sites at 2.3-4.3 km water depth from the equatorial Pacific Ocean has
637 varied by no more than ~15 μmol/kg due to effective buffering effect of the deep-sea $CaCO_3$
638 (Anderson and Archer, 2002).
639
640 (2) Our data suggest that the global mean deep ocean [CO_3^{2-}] is likely similar between the Late
641 Holocene and the LGM. Considering the storage of extra carbon in the deep ocean, the global

642 deep ocean alkalinity (salinity normalized) during the LGM must have been substantially
643 higher than today.
644
645 (3) Our data from the three sites in the Pacific Ocean show temporal rises in deep ocean [CO_3^{2-}]
646 from MIS 5c to mid MIS 3, consistent with a response of the deep ocean carbonate system to
647 a decrease in neritic $CaCO_3$ production associated with ~60 m drop in sea-level (Berger,
648 1982; Opdyke and Walker, 1992).
649
650 (4) The transient changes in [CO_3^{2-}] at MIS 4 observed in our records from the deep Pacific
651 Ocean are consistent with expectation from the vertical nutrient fractionation and carbonate
652 compensation (Boyle, 1988a; Boyle, 1988b; Broecker and Peng, 1987).
653
654 (5) Although sea-level dropped by ~30 m from MIS 3 to the LGM, we see no rise in deep ocean
655 [CO_3^{2-}] over this time interval. The observed decrease in deep water [CO_3^{2-}] at site PC61
656 from 4.3 km water depth in the central Pacific Ocean is consistent with enhanced ocean
657 stratification from the MIS 3 to the LGM (Adkins et al., 2002; Burke and Robinson, 2012;
658 Lund et al., 2011).
659
660 (6) Over the last glacial-interglacial cycle, gradients in [CO_3^{2-}] and $\delta^{13}C$ between the mid-depth
661 North Atlantic (VM28-122) and deep equatorial Pacific (PC61) have varied systematically
662 with atmospheric CO_2 and changed along the biogenic regeneration trend on the [CO_3^{2-}]-$\delta^{13}C$
663 space, lending support to changes in ocean stratification and associated accumulation of

664 respired carbon in the deep ocean as an important factor controlling past atmospheric CO_2
665 variations (Francois et al., 1997; Sigman and Boyle, 2000).
666
667 (7) Covariation of deep water [CO_3^{2-}] and ^{230}Th-normalized $CaCO_3$ flux at two adjacent cores in
668 the central deep Pacific Ocean provides strong support for deep-sea dissolution as a dominant
669 control on past $CaCO_3$ accumulation at these sites (Anderson et al., 2008; Berelson et al.,
670 1997).
671
672
673
674
675 **Acknowledgements:** We thank W.S. Broecker, P. De Deckker, and F.J. Ryerson for helpful
676 discussion, Fei Zhang for assistance with sediment processing and foraminfera picking. Core
677 materials are provided by D. McCorkle at WHOI (MW91-9 GGC15 and MW91-9 GGC48),
678 LDEO core repository (VM28-122), and S. Carey at University of Rhode Island (TTO13 PC61;
679 supported by NSF OCE-644625). We thank the Editor (Dr. Hillaire-Marcel) for editorial
680 handling, and two anonymous reviewers for constructive comments. This research is supported
681 by NSF, LLNL Fellowship, startup fund at RSES-ANU (JY), and by CAS/SAFEA International
682 Partnership Program for Creative Research Teams (JY/ZJ).
683
684

685 **Reference:**

686 Adkins, J.F., McIntyre, K., Schrag, D.P., 2002. The salinity, temperature, and $\delta^{18}O$ of the glacial deep
687 ocean. Science 298, 1769-1773.
688 Anderson, D.M., Archer, D., 2002. Glacial-interglacial stability of ocean pH inferred from foraminifer
689 dissolution rates. Nature 416, 70-73.
690 Anderson, R.F., Ali, S., Bradtmiller, L., Nielsen, S.H.H., Fleisher, M.Q., Anderson, B.E., Burckle, L.H.,
691 2009. Wind-driven upwelling in the Southern Ocean and the deglacial rise in atmospheric CO_2.
692 Science 323, 1443-1448.
693 Anderson, R.F., Fleisher, M.Q., Lao, Y., 2006. Glacial-interglacial variability in the delivery of dust to
694 the central equatorial Pacific Ocean. Earth Planet. Sci. Lett. 242, 406-414. DOI
695 10.1016/j.epsl.2005.11.061
696 Anderson, R.F., Fleisher, M.Q., Lao, Y., Winckler, G., 2008. Modern $CaCO_3$ preservation in equatorial
697 Pacific sediments in the context of late-Pleistocene glacial cycles. Mar. Chem.,
698 doi:10.1016/j.marchem.2007.1011.1011.
699 Archer, D., 1991. Equatorial Pacific calcite preservation cycles: Production or dissolution? Paleoceanogr.
700 6, 561-571.
701 Archer, D., Winguth, A., Lea, D., Mahowald, N., 2000. What caused the glacial/interglacial atmospheric
702 pCO_2 cycles? Reviews of Geophysics 38, 159-189.
703 Arrhenius, G., 1952. Sediment cores from the East Pacific. Part I. Properties of the sediment and their
704 distribution. Rept. Swedish Deep-Sea Expedition 5, 1-90.
705 Barker, S., Archer, D., Booth, L., Elderfield, H., Henderiks, J., Rickaby, R.E.M., 2006. Globally
706 increased pelagic carbonate production during the Mid-Brunhes dissolution interval and the CO2
707 paradox of the MIS 11. Quat. Sci. Rev. 25, 3278-3293. DOI 10.1016/j.quascirev.2006.07.018
708 Barker, S., Greaves, M., Elderfield, H., 2003. A study of cleaning procedures used for foraminiferal
709 Mg/Ca paleothermometry. Geochem. Geophys. Geosyst. 4, 8407. doi:10.1029/2003GC000559
710 Berelson, W.M., Anderson, R.F., Dymond, J., Demaster, D., Hammond, D.E., Collier, R., Honjo, S.,
711 Leinen, M., McManus, J., Pope, R., Smith, C., Stephens, M.P., 1997. Biogenic budgets of particle
712 rain, benthic remineralization and sediment accumulation in the equatorial Pacific. Deep-Sea Res.
713 Part II 44, 2251-2282.
714 Berger, W.H., 1982. Increase of Carbon-Dioxide in the Atmosphere during Deglaciation - the Coral-Reef
715 Hypothesis. Naturwissenschaften 69, 87-88.
716 Bickert, T., Mackensen, A., 2003. Last glacial to Holocene changes in South Atlantic deep water
717 circulation, In: Wefer, G., Mulitza, S., Ratmeyer, V. (Eds.), The South Atlantic in the Late
718 Quaternary: Reconstruction of material budgets and current systems. Springer-Verlag, New York,
719 pp. 671-692.
720 Bird, M.I., Lloyd, J., Farquhar, G.D., 1994. Terrestrial carbon storage at the LGM. Nature 371, 566.
721 Bohonak, A.J., 2004. RMA, software for reduced major axis regression, v1.17.
722 HTTP://WWW.BIO.SDSU.EDU/PUB/ANDY/RMA.HTML.
723 Boyle, E., 1988a. The role of vertical chemical fractionation in controlling late Quaternary atmospheric
724 carbon dioxide. J. Geophys. Res. 93, 15701-15714.
725 Boyle, E.A., 1984. Sampling statistic limitations on benthic foraminifera chemical and isotopic data. Mar.
726 Geol. 58, 213-224.
727 Boyle, E.A., 1988b. Vertical oceanic nutrient fractionation and glacial/interglacial CO_2 cycles. Nature
728 331, 55-56.
729 Boyle, E.A., 1995. Limits on benthic foraminiferal chemical-analyses as precise measures of
730 environmental properties. J. Foraminifer. Res. 25, 4-13.
731 Boyle, E.A., Keigwin, L., 1987. North Atlantic thermohaline circulation during the past 20,000 years
732 linked to high-latitude surface temperature. Nature 330, 35-40.

733 Bradtmiller, L., Anderson, R.F., Sachs, J., Fleisher, M.Q., 2010. A deeper respired carbon pool in the
734 glacial equatorial Pacific Ocean. Earth Planet. Sci. Lett., doi:10.1016/j.epsl.2010.1009.1022.
735 Broecker, W., 1982. Glacial to interglacial changes in ocean chemistry. Progr. Oceanogr. 2, 151-197.
736 Broecker, W., 2008. A need to improve reconstructions of the fluctuations in the calcite compensation
737 depth over the course of the Cenozoic Paleoceanogr. 23, PA1204.
738 Broecker, W.S., Peng, T.H., 1987. The role of $CaCO_3$ compensation in the glacial to interglacial
739 atmospheric CO_2 change. Glob. Biogeochem. Cycle 1, 15-29.
740 Brovkin, V., Ganopolski, A., Archer, D., Rahmstorf, S., 2007. Lowering of glacial atmospheric CO2 in
741 response to changes in oceanic circulation and marine biogeochemistry. Paleoceanogr. 22. Artn
742 Pa4202
743 Doi 10.1029/2006pa001380
744 Brown, S.J., Elderfield, H., 1996. Variations in Mg/Ca and Sr/Ca ratios of planktonic foraminifera caused
745 by postdepositional dissolution: Evidence of shallow Mg- dependent dissolution. Paleoceanogr.
746 11, 543-551.
747 Burke, A., Robinson, L.F., 2012. The Southern Ocean's role in carbon exchange during the last
748 deglaciation. Science, doi:10.1126/science.1208163.
749 Ciais, P., Tagliabue, A., Cuntz, M., Bopp, L., Scholze, M., Hoffmann, G., Lourantou, A., Harrison, S.P.,
750 Prentice, I.C., Kelley, D.I., Koven, C., Piao, S.L., 2012. Large inert carbon pool in the terrestrial
751 biosphere during the Last Glacial Maximum. Nature Geoscience 5, 74-79. Doi 10.1038/Ngeo1324
752 Crowley, T.J., 1983. Calcium-carbonate preservation patterns in the central north-Atlantic during the last
753 150,000 years. Mar. Geol. 51, 1-14.
754 Curry, W.B., Duplessey, J.-C., Labeyrie, L., Shackleton, N.J., 1988. Changes in the distribution of $\delta^{13}C$ of
755 deep water ΣCO_2 between the last glaciation and the Holocene. Paleoceanogr. 3, 317-341.
756 Emerson, S., Archer, D., 1992. Glacial carbonate dissolution cycles and atmospheric pCO_2: A view from
757 the ocean bottom. Paleoceanogr. 7, 319-331.
758 Farrell, J.W., Prell, W.L., 1989. Climatic change and $CaCO_3$ preservation: an 800,000 year bathymetric
759 reconstruction from the central equatorial Pacific Ocean. Paleoceanogr. 4, 447-466.
760 Farrell, J.W., Prell, W.L., 1991. Pacific $CaCO_3$ preservation and $\delta^{18}O$ since 4 Ma: paleoceanic and
761 paleoclimatic implications. Paleoceanogr. 6, 485-498.
762 Foster, G.L., 2008. Seawater pH, pCO_2 and $[CO_3^{2-}]$ variations in the Caribbean Sea over the last 130 kyr;
763 a boron isotope and B/Ca study of planktic foraminifera. Earth Planet. Sci. Lett. 271, 254-266.
764 doi: 210.1016/j.epsl.2008.1004.1015.
765 Foster, G.L., Ni, Y., Haley, B., Elliott, T., 2006. Accurate and precise isotopic measurement of sub-
766 nanogram sized samples of foraminiferal hosted boron by total evaporation NTIMS. Chem. Geol.
767 230, 161-174.
768 Francois, R., Altabet, M.A., Yu, E.F., Sigman, D.M., Bacon, M.P., Frank, M., Bohrmann, G., Bareille, G.,
769 Labeyrie, L.D., 1997. Contribution of Southern Ocean surface-water stratification to low
770 atmospheric CO2 concentrations during the last glacial period. Nature 389, 929-935.
771 10.1038/40073
772 Gibbs, M.T., Kump, L.R., 1994. Global chemical erosion during the last glacial maximum and the
773 present: Sensitivity to changes in lithology and hydrology. Paleoceanogr. 9, 529-543.
774 Grant, K.M., Rohling, E.J., Bar-Matthews, M., Ayalon, A., Medina-Elizalde, M., Bronk Ramsey, C.,
775 Satow, C., Roberts, A.P., 2012. Rapid coupling between ice volume and polar temperature over
776 the past 150,000 years. Nature, doi:10.1038/nature11593.
777 Hain, M.P., Sigman, D.M., Haug, G.H., 2010. Carbon dioxide effects of Antarctic stratification, North
778 Atlantic Intermediate Water formation, and subantarctic nutrient drawdown during the last ice
779 age: Diagnosis and synthesis in a geochemical box model. Glob. Biogeochem. Cycle 24.
780 10.1029/2010gb003790
781 Hain, M.P., Sigman, D.M., Haug, G.H., 2013. The Biological Pump in the Past, Treatise on Geochemsitry
782 2nd edition, pp. doi: 10.1016/B1978-1010-1008-095975-095977.000618-095975.

783 Henehan, M.J., Rae, J., Foster, G.L., Erez, J., Prentice, K.C., Kucera, M., Bostock, H.C., Martinez-Boti,
784 M.A., Milton, J.A., Wilson, P.A., Marshall, B.J., Elliott, T., 2013. Calibration of the boron isotope
785 proxy in the planktonic foraminifera *Globigerinoides ruber* for useinpalaeo-CO_2 reconstruction.
786 Earth Planet. Sci. Lett. 364, 111-122.
787 Herguera, J.C., Herbert, T., Kashgarian, M., Charles, C., 2010. Intermediate and deep water mass
788 distribution in the Pacific during the Last Glacial Maximum inferred from oxygen and carbon
789 stable isotopes. Quat. Sci. Rev. 29, 1228-1245. DOI 10.1016/j.quascirev.2010.02.009
790 Hodell, D.A., Charles, C.D., Sierro, F.J., 2001. Late Pleistocene evolution of the ocean's carbonate
791 system. Earth Planet. Sci. Lett. 192, 109-124.
792 Hodell, D.A., Venz, K.A., Charles, C.D., Ninnemann, U.S., 2003. Pleistocene vertical carbon isotope and
793 carbonate gradients in the South Atlantic sector of the Southern Ocean. Geochem. Geophys.
794 Geosyst. 4, doi:10.1029/2002GC000367.
795 Hönisch, B., Bickert, T., Hemming, N.G., 2008. Modern and Pleistocene boron isotope composition of
796 the benthic foraminifer *Cibicidoides wuellerstorfi*. Earth Planet. Sci. Lett. 272, 309-318. doi:
797 310.1016/j.epsl.2008.1004.1047.
798 Howard, W.R., Prell, W.L., 1994. Late Quaternary $CaCO_3$ production and preservation in the Southern
799 Ocean - Implications for oceanic and atmospheric carbon cycling. Paleoceanogr. 9, 453-482.
800 Jaccard, S.L., Galbraith, E.D., Sigman, D.M., Haug, G.H., Francois, R., Pedersen, T.F., Dulski, P.,
801 Thierstein, H.R., 2009. Subarctic Pacific evidence for a glacial deepening of the oceanic respired
802 carbon pool. Earth Planet. Sci. Lett. 277, 156-165.
803 Keigwin, L., 1998. Glacial-age hydrography of the far northwest Pacific Ocean. Paleoceanogr. 13, 323-
804 339.
805 Key, R.M., Kozyr, A., Sabine, C.L., Lee, K., Wanninkhof, R., Bullister, J.L., Feely, R.A., Millero, F.J.,
806 Mordy, C., Peng, T.H., 2004. A global ocean carbon climatology: Results from Global Data
807 Analysis Project (GLODAP). Glob. Biogeochem. Cycle 18. 10.1029/2004GB002247
808 Kohfeld, K.E., Le Quere, C., Harrison, S.P., Anderson, R.F., 2005. Role of marine biology in glacial-
809 interglacial CO2 cycles. Science 308, 74-78. 10.1126/science.1105375
810 Kumar, N., Anderson, R.F., Mortlock, R.A., Froelich, P.N., Kubik, P., Dittrichhannen, B., Suter, M.,
811 1995. Increased Biological Productivity and Export Production in the Glacial Southern-Ocean.
812 Nature 378, 675-680. Doi 10.1038/378675a0
813 Kwon, E.Y., Hain, M.P., Sigman, D.M., Galbraith, E.D., Sarmiento, J.L., Toggweiler, J.R., 2012. North
814 Atlantic ventilation of "southern-sourced" deep water in the glacial ocean. Paleoceanogr. 27.
815 10.1029/2011pa002211
816 Lambert, F., Delmonte, B., Petit, J.R., Bigler, M., Kaufmann, P.R., Hutterli, M.A., Stocker, T.F., Ruth,
817 U., Steffensen, J.P., Maggi, V., 2008. Dust-climate couplings over the past 800,000 years from the
818 EPICA Dome C ice core. Nature 452, 616-619. Doi 10.1038/Nature06763
819 Le, J., Shackleton, N.J., 1992. Carbonate dissolution fluctuations in the Western equatorial Pacific during
820 the late Quaternary. Paleoceanogr. 7, 21-42.
821 Lea, D., Bijam, J., Spero, H., Archer, D., 1999. Implications of a carbonate ion effect on shell carbon and
822 oxygen isotopes for glacial ocean conditions, In: Fischer, G., Wefer, G. (Eds.), Use of Proxies in
823 Paleoceanography: Examples from the South Atlantic. Springer-Verlag, Berlin Heidelberg, pp.
824 513-522.
825 Leduc, G., Vidal, L., Tachikawa, K., Bard, E., 2010. Changes in Eastern Pacific ocean ventilation at
826 intermediate depth over the last 150 kyr BP. Earth Planet. Sci. Lett. 298, 217-228. DOI
827 10.1016/j.epsl.2010.08.002
828 Lemarchand, D., Gaillardet, J., Lewin, E., Allegre, C.J., 2000. The influence of rivers on marine boron
829 isotopes and implications for reconstructing past ocean pH. Nature 408, 951-954.
830 Lippod, J., Luo, Y., Francois, R., ALlen, S.E., Gherardi, J.M., Pichat, S., Hickey, B., Schulz, H., 2012.
831 Strength and geometry of the glacial Atlantic Meridional Overturning Circulation. Nature
832 Geoscience. 10.1038/NGEO1608

833 Lisiecki, L.E., Raymo, M.E., 2005. A Pliocene-Pleistocene stack of 57 globally distributed benthic $\delta^{18}O$
834 records. Paleoceanogr. 20, PA1003, doi:1010.1029/2004PA001071.
835 Lund, D.C., Adkins, J.F., Ferrari, R., 2011. Abyssal Atlantic circulation during the Last Glacial
836 Maximum: Constraining the ratio between transport and vertical mixing. Paleoceanogr. 26.
837 10.1029/2010pa001938
838 Lüthi, D., Floch, M.L., Bereiter, B., Blunier, T., Barnola, J.M., Siegenthaler, U., Raynaud, D., Jouzel, J.,
839 Fischer, H., Kawamura, K., Stocker, T.F., 2008. High-resolution carbon dioxide concentration
840 record 650,000–800,000 years before present. Nature 453, doi:10.1038/nature06949.
841 Lyle, M., Mix, A.C., Ravelo, A.C., Andreasen, D., Heuser, L., Olivarez, A., 2000. Millennial-scale
842 $CaCO_3$ and C_{org} events along the Northern and central California margins: stratigraphy and
843 origins, In: Lyle, M., Koizumi, I., Richter, C., Moore, T.C. (Eds.), Proceedings of the Ocean
844 Drilling Program, Scientific Results, pp. 163-182.
845 Lyle, M., Zahn, R., Prahl, F., Dymond, J., Collier, R., Pisias, N., Suess, E., 1992. Paleoproductivity and
846 Carbon Burial across the California Current: The Multitracers Transect, 42 Degrees N.
847 Paleoceanogr. 7, 251-272. 10.1029/92pa00696
848 Marcantonio, F., Anderson, R.F., Higgins, S., Stute, M., Schlosser, P., Kubik, P., 2001. Sediment
849 focusing in the central equatorial Pacific Ocean. Paleoceanogr. 16, 260-267. Doi
850 10.1029/2000pa000540
851 Marchitto, T.M., Curry, W.B., Oppo, D.W., 2000. Zinc concentrations in benthic foraminifera reflect
852 seawater chemistry. Paleoceanogr. 15, 299-306.
853 Marchitto, T.M., Lynch-Stieglitz, J., Hemming, S.R., 2005. Deep Pacific $CaCO_3$ compensation and
854 glacial-interglacial atmospheric CO_2. Earth Planet. Sci. Lett. 231, 317-336.
855 Marchitto, T.M., Oppo, D.W., Curry, W.B., 2002. Paired benthic foraminiferal Cd/Ca and Zn/Ca
856 evidence for a greatly increased presence of Southern Ocean Water in the glacial North Atlantic.
857 Paleoceanogr. 17, doi:10.1029/2000PA000598.
858 Martinez-Garcia, A., Rosell-Mele, A., Jaccard, S.L., Geibert, W., Sigman, D.M., Haug, G.H., 2011.
859 Southern Ocean dust-climate coupling over the past four million years. Nature 476, 312-U141.
860 Doi 10.1038/Nature10310
861 Matsumoto, K., Oba, T., Lynch-Stieglitz, J., Yamamoto, H., 2002. Interior hydrography and circulation of
862 the glacial Pacific Ocean. Quat. Sci. Rev. 21, 1693-1704.
863 McCave, I.N., Carter, L., Hall, I.R., 2008. Glacial-interglacial changes in water mass structure and flow in
864 the SW Pacific Ocean. Quat. Sci. Rev. 27, 1886-1908. 10.1016/j.quascirev.2008.07.010
865 McCave, I.N., Kiefer, T., Thornalley, D.J.R., Elderfield, H., 2005. Deep flow in the Madagascar-
866 Mascarene Basin over the last 150 000 years. Philos. Trans. R. Soc. Lond. Ser. A-Math. Phys.
867 Eng. Sci. 363, 81-99.
868 Menviel, L., Joos, F., 2012. Toward explaining the Holocene carbon dioxide and carbon isotope records:
869 Results from transient ocean carbon cycle-climate simulations. Paleoceanogr. 27.
870 10.1029/2011pa002224
871 Menviel, L., Joos, F., Ritz, S.P., 2012. Simulating atmospheric CO_2, ^{13}C and the marine carbon cycle
872 during the Last Glaciale/Interglacial cycle: possible role for a deepening of the mean
873 remineralization depth and an increase in the oceanic nutrient inventory. Quat. Sci. Rev. 56, 46-
874 68.
875 Milliman, J.D., 1974. Marine Carbonates. Springer-Verlag, New York.
876 Milliman, J.D., 1993. Production and Accumulation of Calcium-Carbonate in the Ocean - Budget of a
877 Nonsteady State. Glob. Biogeochem. Cycle 7, 927-957. Doi 10.1029/93gb02524
878 Mix, A.C., 2001. Final d18O_d13C versus age, Site 849,. PANGAEA, p. doi:10.1594/PANGAEA.60261.
879 Opdyke, B.N., Walker, J.C.G., 1992. Return of the Coral-Reef Hypothesis - Basin to Shelf Partitioning of
880 $CaCO_3$ and Its Effect on Atmospheric CO_2. Geology 20, 733-736.
881 Oppo, D., Fairbanks, R.G., 1990. Atlantic Ocean thermohaline circulation of the last 150,000 years:
882 Relationship to climate and atmospheric CO_2. Paleoceanogr. 5, 277-288.

Oppo, D.W., Lehman, S.J., 1993. Mid-depth circulation of the subpolar North Atlantic during the last glacial maximum. Science 259, 1148-1152.
Paytan, A., Kastner, M., Chavez, F.P., 1996. Glacial to interglacial fluctuations productivity in the equatorial Pacific indicated by marine barite. Science 274, 1355-1357.
Rae, J.W.B., Foster, G.L., Schmidt, D.N., Elliott, T., 2011. Boron isotopes and B/Ca in benthic foraminifera: Proxies for the deep ocean carbonate system. Earth Planet. Sci. Lett. 302, 403-413. 10.1016/j.epsl.2010.12.034
Raitzsch, M., Hathorne, E.C., Kuhnert, H., Groeneveld, J., Bickert, T., 2011. Modern and late Pleistocene B/Ca ratios of the benthic foraminifer Planulina wuellerstorfi determined with laser ablation ICP-MS. Geology 39, 1039-1042. 10.1130/G32009.1
Ribbat, B., Roether, W., Münnich, K.O., 1976. Turnover of Eastern Caribbean deep water from ^{14}C measurements. Earth Planet. Sci. Lett. 32, 331-341.
Rickaby, R.E.M., Elderfield, H., Roberts, N., Hillenbrand, C.-D., Mackensen, A., 2010. Evidence for elevated alkalinity in the glacial Southern Ocean. Paleoceanogr. 25, PA1209, doi:1210.1029/2009PA001762.
Ridgwell, A.J., Kennedy, M.J., Caldeira, K., 2003a. Carbonate deposition, climate stability, and neoproterozoic ice ages. Science 302, 859-862.
Ridgwell, A.J., Watson, A.J., Maslin, M.A., Kaplan, J.O., 2003b. Implications of coral reef buildup for the controls on atmospheric CO_2 since the Last Glacial Maximum. Paleoceanogr. 18. 10.1029/2003PA000893
Robinson, R.S., Sigman, D.M., 2008. Nitrogen isotopic evidence for a poleward decrease in surface nitrate within the ice age Antarctic. Quat. Sci. Rev. 27, 1076-1090. DOI 10.1016/j.quascirev.2008.02.005
Ruddiman, W.F., Raymo, M.E., Martinson, D.G., Clement, B.M., Backman, J., 1989. Pleistocene Evolution: Northern Hemisphere Ice Sheets and North Atlantic Ocean. Paleoceanogr. 4, 353-412. Doi 10.1029/Pa004i004p00353
Sanyal, A., Hemming, N.G., Hanson, G.N., Broecker, W.S., 1995. Evidence for a higher pH in the glacial ocean from boron isotopes in foraminifera. Nature 373, 234-236.
Schlitzer, R., 2006. Ocean Data View. http://odv.awi-bremerhaven.de.
Sigman, D.M., Boyle, E.A., 2000. Glacial/interglacial variations in atmospheric carbon dioxide. Nature 407, 859-869.
Sigman, D.M., Hain, M.P., Haug, G.H., 2010. The polar ocean and glacial cycles in atmospheric CO_2 concentration. Nature 466, 47-55. 10.1038/Nature09149
Sortor, R.N., Lund, D.C., 2011. No evidence for a deglacial intermediate water Delta C-14 anomaly in the SW Atlantic. Earth Planet. Sci. Lett. 310, 65-72. DOI 10.1016/j.epsl.2011.07.017
Thompson, W.G., Goldstein, S.L., 2006. A radiometric calibration of the SPECMAP timescale. Quat. Sci. Rev. 25, 3207-3215. DOI 10.1016/j.quascirev.2006.02.007
Toggweiler, J.R., 2008. Origin of the 100,000-year timescale in Antarctic temperatures and atmospheric CO_2. Paleoceanogr. 23, PA2211, doi:2210.1029/2006PA001405.
Waelbroeck, C., Labeyrie, L., Michel, E., Duplessy, J.C., McManus, J.F., Lambeck, K., Balbon, E., Labracherie, M., 2002. Sea-level and deep water temperature changes derived from benthic foraminifera isotopic records. Quat. Sci. Rev. 21, 295-305.
Yu, J., Broecker, W., Elderfield, H., Jin, Z.D., McManus, J., Zhang, F., 2010a. Loss of carbon from the deep sea since the Last Glacial Maximum. Science 330, 1084-1087, doi: 1010.1126/science.1193221.
Yu, J., Elderfield, H., Greaves, M., Day, J., 2007. Preferential dissolution of benthic foraminiferal calcite during laboratory reductive cleaning. Geochem. Geophys. Geosyst. 8, doi:10.1029/2006gc001571.
Yu, J., Foster, G.L., Elderfield, H., Broecker, W.S., Clark, E., 2010b. An evaluation of benthic foraminiferal B/Ca and delta(11)B for deep ocean carbonate ion and pH reconstructions. Earth Planet. Sci. Lett. 293, 114-120. 10.1016/j.epsl.2010.02.029

933 Yu, J., Thornalley, D.J.R., Rae, J., McCave, I.N., 2013. Calibration and application of B/Ca, Cd/Ca, and
934 $\delta^{11}B$ in *Neogloboquadrina pachyderma* (sinistral) to constrain CO_2 uptake in the subpolar North
935 Atlantic during the last deglaciation. Paleoceanogr. 10.1002/palo.20024
936 Yu, J.M., Day, J., Greaves, M., Elderfield, H., 2005. Determination of multiple element/calcium ratios in
937 foraminiferal calcite by quadrupole ICP-MS. Geochem. Geophys. Geosyst. 6, Q08P01,
938 doi:10.1029/2005GC000964.
939 Yu, J.M., Elderfield, H., 2007. Benthic foraminiferal B/Ca ratios reflect deep water carbonate saturation
940 state. Earth Planet. Sci. Lett. 258, 73-86, doi: 10.1016/j.epsl.2007.1003.1025.
941 Yu, J.M., Elderfield, H., Piotrowski, A., 2008. Seawater carbonate ion-$\delta^{13}C$ systematics and application to
942 glacial-interglacial North Atlantic ocean circulation. Earth Planet. Sci. Lett. 271, 209-220.
943 doi:210.1016/j.epsl.2008.1004.1010.
944 Zeebe, R.E., Marchitto, T.M., 2010. Atmosphere and ocean chemistry. Nature Geoscience 3, 386-387.
945
946

Tables

Table 1. Core locations together with deep water $[CO_3^{2-}]$ and $[CO_3^{2-}]_{sat}$ (μmol/kg) above these sites (Key et al., 2004).

Core	Latitude	Longitude	Water depth	$[CO_3^{2-}]_{preindustrial}$	$[CO_3^{2-}]_{sat}$
VM28-122	12°N	79°W	3623 m†	106	86
GGC15	0°N	58°E	2311 m	73	67
GGC48	0°N	161°E	3400 m	78	83
PC61	0.86°S	140°W	4276 m	80	98

†: sill depth is 1800 m.

974 **Table 2**. Average deep water [CO_3^{2-}] for selected time intervals and differences between them at
975 the four studied sites. Errors represent 1 standard deviation of reconstructions within the
976 indicated time interval.

Core	Deep water [CO_3^{2-}] (μmol/kg)						Difference (μmol/kg)			
	Late HOL	LGM	mid MIS 3	MIS 5c	MIS 5e	mid MIS 6	LGM - Late HOL	MIS 6 - MIS5e	MIS 5e – Late HOL	MIS 5c - mid MIS 3
	0-5 ka	19-23 ka	36-45 ka	93-105 ka	115-130 ka	135-145 ka				
VM28-122	111±4 (2)[§]	145±5 (4)	138±6(8)	122±7(11)	105±7 (6)	135±15 (4)	34±6	30±17	-6±8	-16±9
GGC15	70±2 (3)	73±2 (3)	72±2(5)	65±4(7)	66±4 (4)	73±2 (7)	3±3	7±4	-4±4	-7±4
GGC48	79±2 (2)	74±2 (3)	78±3(11)	70±3(10)	–	–	-5±3	–	–	-8±4
PC61	86±4 (8)[*]	87±3 (3)	91±5(13)	84±4(2)	75±2 (4)	82±2 (4)	1±4	7±3	-10±4	-7±6

977 [§]: number of samples used for averaging; [*]: for the time interval <8 ka.
978
979
980
981
982
983
984

985 **Figure captions**

986 **Fig. 1**. Locations of cores used in this study in the context of pre-industrial seawater [CO_3^{2-}]
987 based on the GLODAP dataset (Key et al., 2004). Core VM28-122 is plotted at the sill depth of
988 1.8 km of Caribbean Basin (Table 1). Inset shows the hydrographic transect used to generate the
989 bathymetric profile of [CO_3^{2-}]. Profile and map are generated using ODV (Schlitzer, 2006).
990 NADW: North Atlantic Deep Water; LCDW: Lower Circumpolar Deep Water; NPDW: North
991 Pacific Deep Water. The reader is referred to the web version of this article for colour figures.
992

993 **Fig. 2.** Age models and sedimentation rates of four studied cores. The ages of cores are based on
994 radiocarbon dates at <~30 ka (crosses) and visual comparison of benthic $\delta^{18}O$ (triangles) with the
995 global benthic $\delta^{18}O$ stack curve (grey curves) (Lisiecki and Raymo, 2005). In (**D**), *Pulleniatina*
996 *obliquiloculata* $\delta^{18}O$ (empty diamonds) is shifted by +3.5‰ to place the record in the same range
997 as benthic $\delta^{18}O$. With the exception of GGC48 during ~150-120 ka which is likely compromised
998 by bioturbation (dark grey triangles), all cores capture expected glacial-interglacial structures in
999 $\delta^{18}O$. Data sources: radiocarbon dates for PC61 are from this study (Supplementary Materials)
1000 and others are from (Yu et al., 2010a); $\delta^{18}O$ at <~30 ka in VM28-122 are from (Oppo and
1001 Fairbanks, 1990), $\delta^{18}O$ at <50 ka in GGC15 and GGC48 from (Yu et al., 2010a), and all others
1002 from this study (Supplementary Materials). The reader is referred to the web version of this
1003 article for colour figures.
1004

1005 **Fig. 3. (A)** Calibration of core-top B/Ca against pre-industrial deep water $\Delta[CO_3^{2-}]$ for two
1006 epifaunal benthic foraminifera *C. wuellerstorfi* and *C. mundulus*. Core-top data are from five
1007 studies (Brown and Elderfield, 1996; Rae et al., 2011; Raitzsch et al., 2011; Yu and Elderfield,

2007; this study). Altogether, 7 B/Ca in *C. wullerstorfi* and 1 B/Ca in *C. mundulus* are judged as outliers and are excluded, due to possible laboratory contamination based on replicate analyses (Yu and Elderfield, 2007), high Al/Ca (Rae et al., 2011), and anomalous morphology of foraminiferal shells (Rae et al., 2011). The regressions shown are for all B/Ca replicates. If B/Ca averages are used, the regressions are: $y = 1.16\pm0.04x + 176.5\pm1.2$, n=152, $R^2 = 0.86$, $P<0.0001$ for *C. wuellerstorfi* and $y = 0.67\pm0.04x + 122.1\pm2.0$, n= 48, $R^2=0.84$, $P<0.0001$ for *C. mundulus*. The intercepts and slopes are indistinguishable from those based on the regression on all replicates (shown in Fig. 3) and from previous estimates (Raitzsch et al., 2011; Yu and Elderfield, 2007). Uncertainties associated with slopes and intercepts are standard errors. (**B**) locations of core-top samples (circles: *C. wuellerstorfi*, squares: *C. mundulus*). Map generated by ODV (Schlitzer, 2006). Data are presented in supplementary Materials. The reader is referred to the web version of this article for colour figures.

Fig. 4. *C. wuellerstorfi* B/Ca of four studied cores. Grey symbols represent B/Ca replicates. In (**C**), empty triangles indicate samples probably biased by bioturbation (Fig. 2C) and these B/Ca are not plotted in other figures. Data sources: B/Ca in VM28-122 are from (Yu et al., 2010b), B/Ca at <50 ka in GGC15 and GGC48 from (Yu et al., 2010a), and all others from this study (Supplementary Materials). The reader is referred to the web version of this article for colour figures.

Fig. 5. Vertical distribution of deep water [CO_3^{2-}] in the North Atlantic (circles) and Indo-Pacific (triangles) Oceans during the Late Holocene (Late HOL; solid symbols) and the LGM (open symbols). Data for the North Atlantic profile are based on VM28-122 (Table 2) and 6 cores

1031 presented in (Yu et al., 2008), while those for the Indo-Pacific profile are based on WIND 28K
1032 from the Indian Ocean (Yu et al., 2010a) and three cores from the Pacific Ocean (Table 2). The
1033 water depths of cores are adjusted by -120 m during the LGM. Compared to the North Atlantic
1034 Ocean, the Indo-Pacific Oceans witnessed relatively small changes in deep water [CO_3^{2-}]. The
1035 reader is referred to the web version of this article for colour figures.
1036
1037 **Fig. 6.** Deep water [CO_3^{2-}] and $\delta^{13}C$ of four studied cores (**A**-**H**) compared with the global sea
1038 level change (Grant et al., 2012; Thompson and Goldstein, 2006; Waelbroeck et al., 2002) (**I**)
1039 and atmospheric CO_2 (Lüthi et al., 2008) (**J**) during the last 160 ka. Deep water [CO_3^{2-}] are
1040 derived from B/Ca shown in Fig. 4 and only average [CO_3^{2-}] with 1SD error bars are shown for
1041 clarification. Black and red arrows show the long-term trends and transient changes,
1042 respectively. Benthic $\delta^{13}C$ data sources: $\delta^{13}C$ at <30 ka in VM28-122 are from (Oppo and
1043 Fairbanks, 1990), $\delta^{13}C$ at <50 ka in GGC15 and GGC48 from (Yu et al., 2010a), and others from
1044 this study (Supplementary Materials). The reader is referred to the web version of this article for
1045 colour figures.
1046
1047 **Fig. 7**. Schematic diagram showing responses of deep ocean [CO_3^{2-}], $\delta^{13}C$, whole ocean
1048 alkalinity, and atmospheric CO_2 to (**A**) sea level changes and (**B**) ocean vertical carbon
1049 fractionation. No scales are given to either axis, and thus the changes are only qualitative to
1050 assistant understanding the deep ocean carbonate system. The horizontal grey lines represent the
1051 long-term steady state values. In (**A**), it is assumed that the growth of coral reefs on shelves are
1052 coupled with sea level changes at all times: when sea-level drops neritic $CaCO_3$ production
1053 decreases and vice versa. While this may be reasonable during most of times at marine

regressions since corals die as sea level drops, a lag in the coral reef growth with respect to the sea level rise is expected at deglaciations due to the fact that coral growth cannot catch up the rate of the sea level rise at transgressions. Dashed curves shown in (**A**) show delayed responses of deep ocean [CO_3^{2-}], oceanic alkalinity, and atmospheric CO_2. Deep ocean alkalinity and [CO_3^{2-}] are expected to change at a ratio of 2:1 in scenario (**A**), while no overall correlation is expected between them in scenario (**B**). In each scenario of **A** and **B**, other factors affecting deep ocean [CO_3^{2-}] such as ALK inputs from rivers and pelagic $CaCO_3$ production are assumed constant. Mechanisms causing changes in ocean ALK in scenarios **A** and **B** are different. In **A**, a change in ocean ALK is a response to changes in the production and burial of $CaCO_3$ on continental shelves. In **B**, a change in ocean ALK is a response to changes in preservation of $CaCO_3$ in deep-sea sediments, forced by variable levels of respiratory CO_2. G: glacial; IG: interglacial; dg: deglacial. The reader is referred to the web version of this article for colour figures.

Fig. 8. Benthic $\delta^{13}C$ from the global deep ocean showing significant changes by ~0.5-1.5‰ at the start and end of MIS 4 (Hodell et al., 2003; McCave et al., 2005; Mix, 2001; Ruddiman et al., 1989). The reader is referred to the web version of this article for colour figures.

Fig. 9. Comparison of gradients in deep water [CO_3^{2-}] (**A**) and $\delta^{13}C$ (**B**) between cores VM28-122 and PC61 with atmospheric CO_2 during the last 160 ka (Lüthi et al., 2008). To difference records between the two cores, [CO_3^{2-}] and $\delta^{13}C$ at site VM28-122 are firstly interpolated at the resolution of PC61 (Supplementary Materials). (**C**) Correlation of [CO_3^{2-}] and $\delta^{13}C$ gradients compared with the biogenic regeneration trend (green) (Yu et al., 2008). The best linear fit (red)

of data in (**C**) is based on reduced major axis regression (Bohonak, 2004). The reader is referred to the web version of this article for colour figures.

Fig. 10. Comparison of %$CaCO_3$ (**A**) ^{230}Th-normalized $CaCO_3$ flux and deep water [CO_3^{2-}] (**B**) at two adjacent cores PC61 (this study; Supplementary Materials) and PC72 (0.1137°N, 139.4015°W, 4298 m water depth) (Anderson et al., 2008) from the central deep Pacific Ocean during the last 160 ka. Overall, deep water [CO_3^{2-}] and ^{230}Th-normalized $CaCO_3$ flux show similar patterns during the last glacial-interglacial cycle. The reader is referred to the web version of this article for colour figures.

Figures

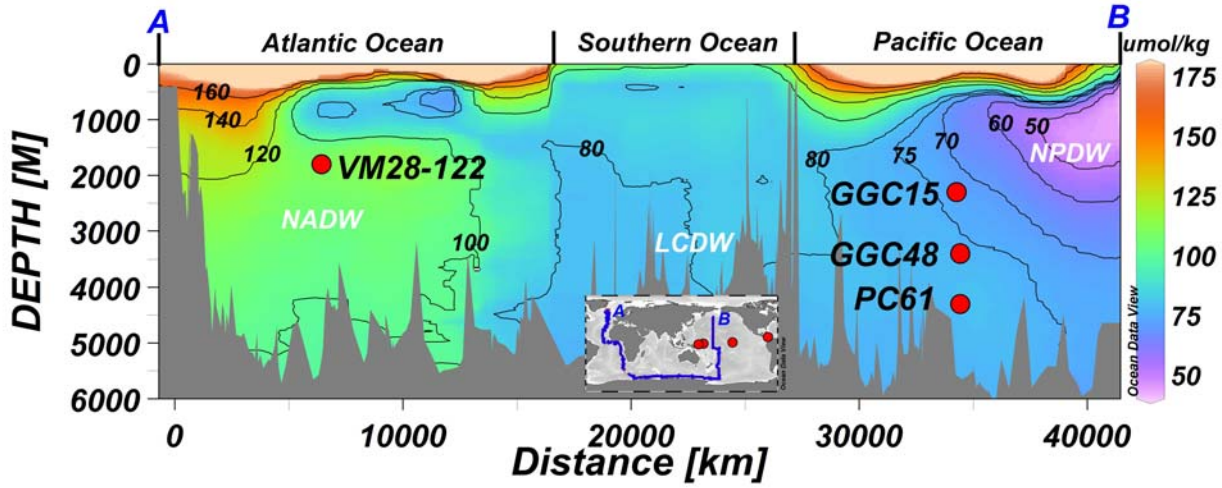

Fig. 1.

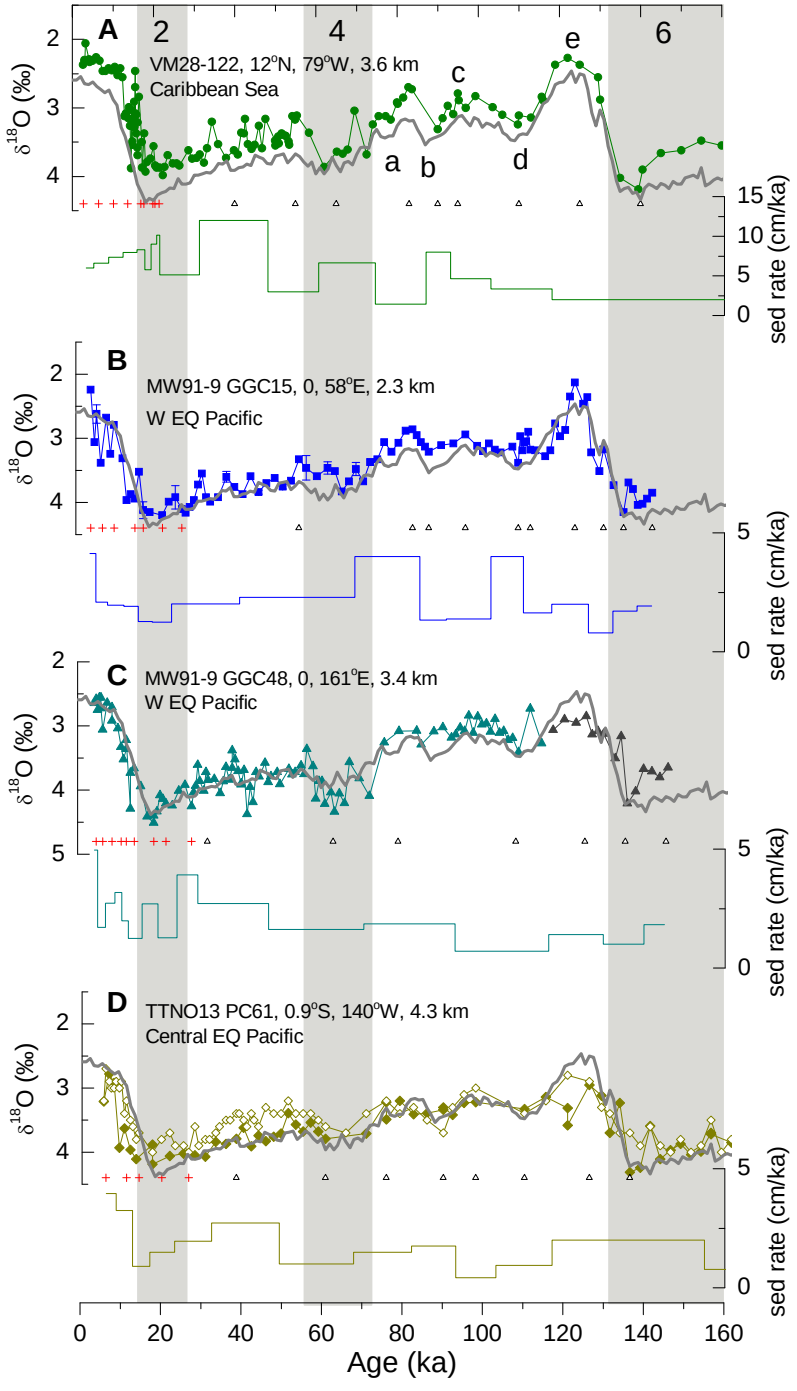
A
2
4
6
VM28-122, 12°N, 79°W, 3.6 km
Caribbean Sea
a
b
c
d
e
δ18O (‰)
sed rate (cm/ka)
B
MW91-9 GGC15, 0, 58°E, 2.3 km
W EQ Pacific
C
MW91-9 GGC48, 0, 161°E, 3.4 km
W EQ Pacific
D
TTNO13 PC61, 0.9°S, 140°W, 4.3 km
Central EQ Pacific
Age (ka)

Fig. 2.

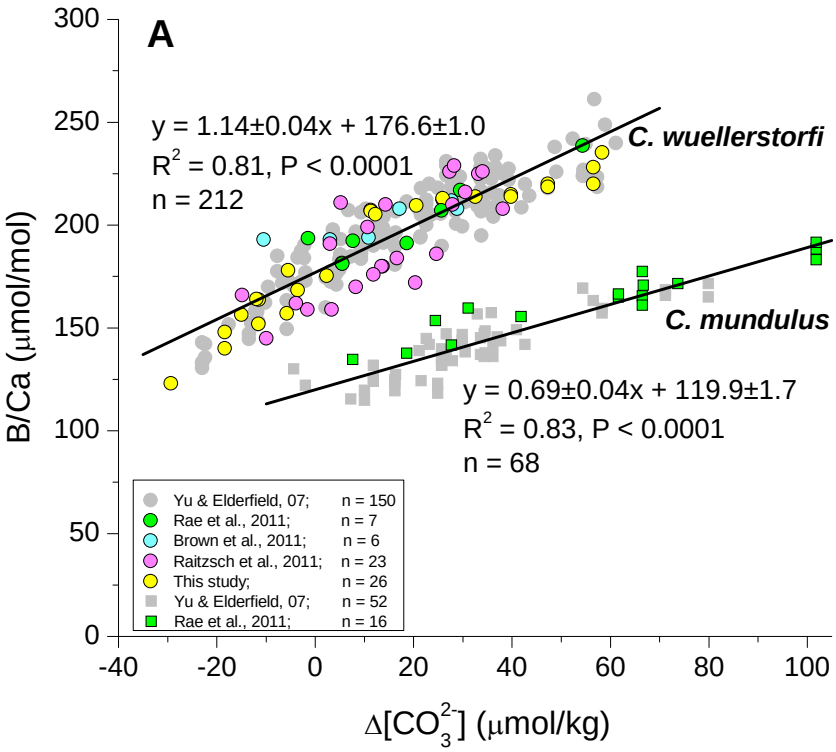
A
y = 1.14±0.04x + 176.6±1.0
R2 = 0.81, P < 0.0001
n = 212
C. wuellerstorfi
C. mundulus
y = 0.69±0.04x + 119.9±1.7
R2 = 0.83, P < 0.0001
n = 68
Yu & Elderfield, 07; n = 150
Rae et al., 2011; n = 7
Brown et al., 2011; n = 6
Raitzsch et al., 2011; n = 23
This study; n = 26
Yu & Elderfield, 07; n = 52
Rae et al., 2011; n = 16
B/Ca (μmol/mol)
Δ[CO32-] (μmol/kg)
300
250
200
150
100
50
0
-40
-20
0
20
40
60
80
100

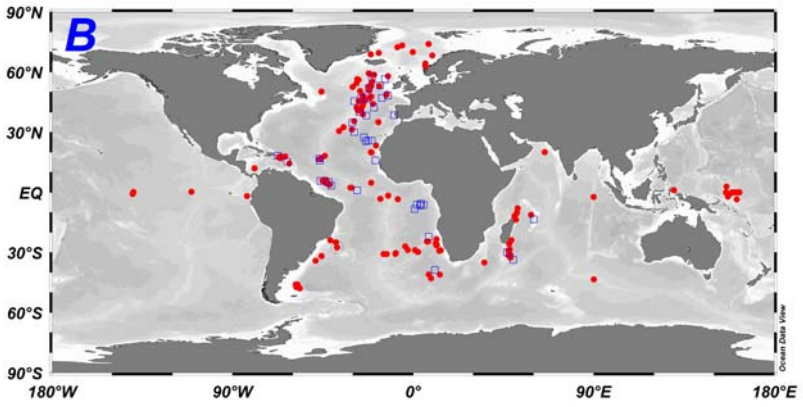
B
90°N
60°N
30°N
EQ
30°S
60°S
90°S
180°W
90°W
0°
90°E
180°E

Fig. 3.

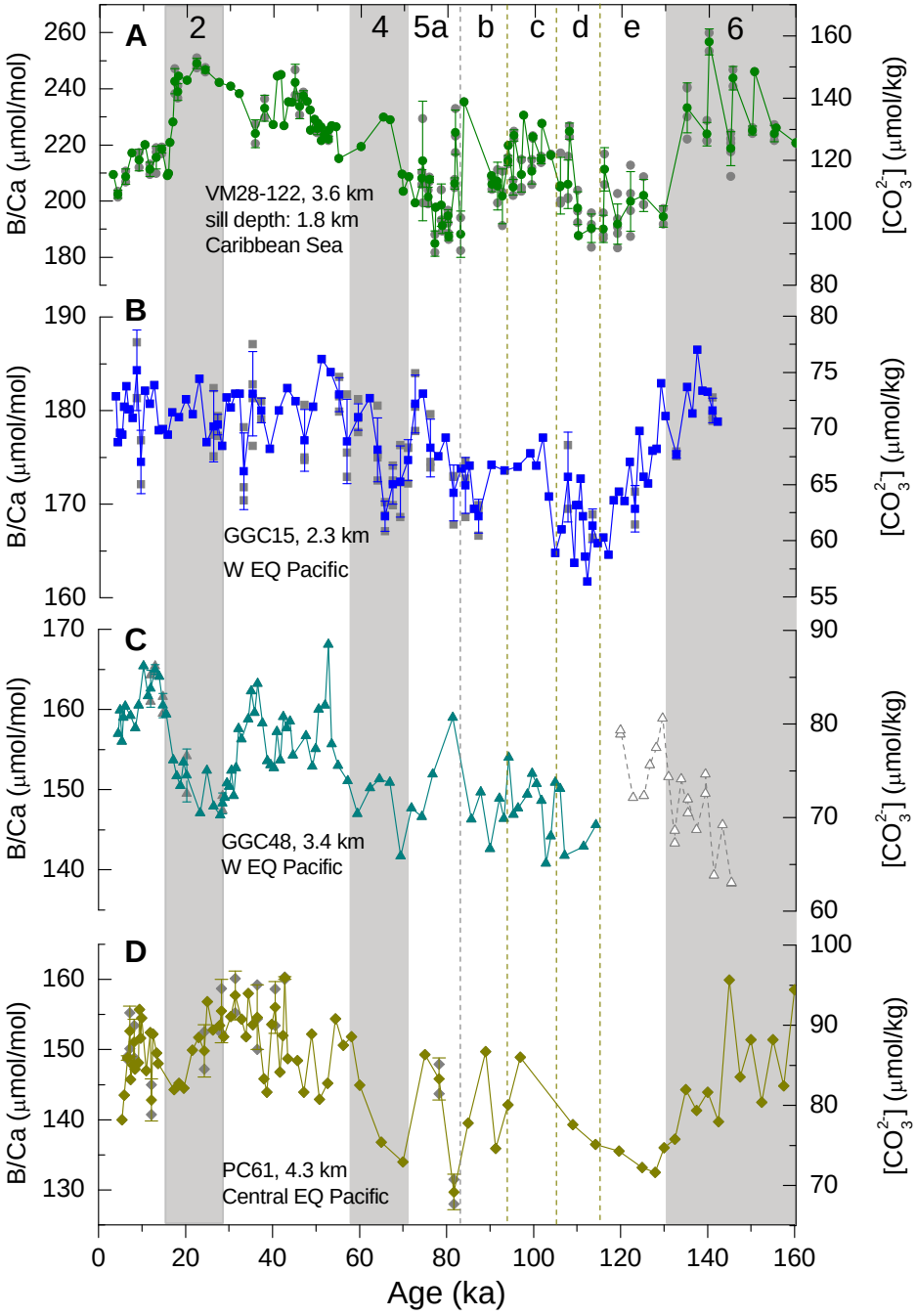
A
B
C
D
2
4
5a
b
c
d
e
6
VM28-122, 3.6 km
sill depth: 1.8 km
Caribbean Sea
GGC15, 2.3 km
W EQ Pacific
GGC48, 3.4 km
W EQ Pacific
PC61, 4.3 km
Central EQ Pacific
B/Ca (µmol/mol)
[CO3 2-] (µmol/kg)
Age (ka)

Fig. 4.

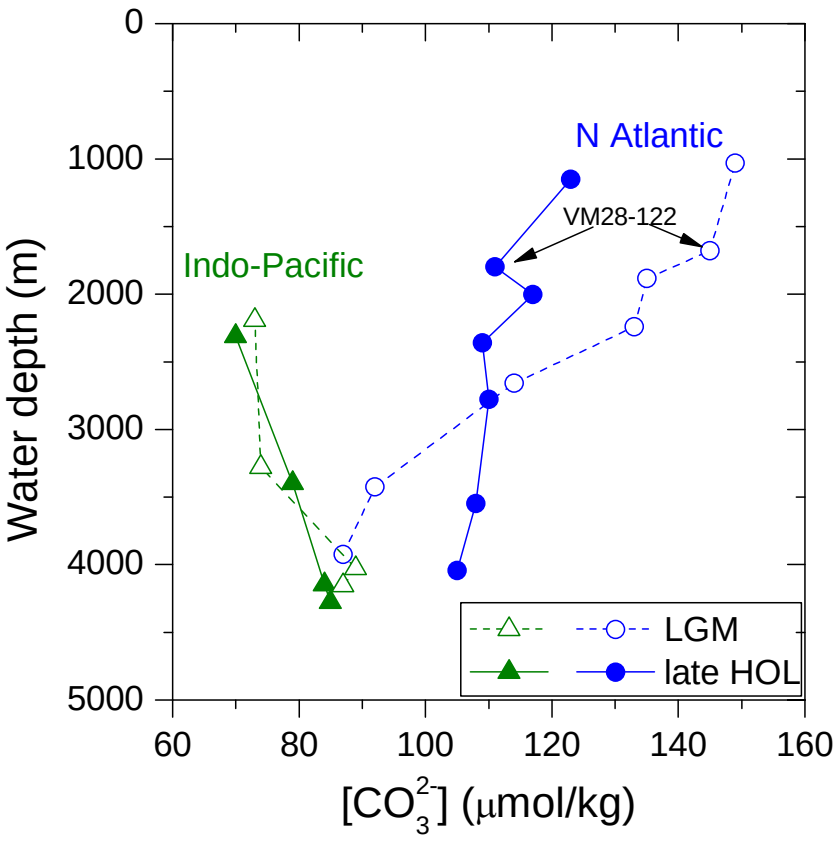
0
1000
2000
3000
4000
5000
Water depth (m)
60
80
100
120
140
160
[CO3 2-] (μmol/kg)
N Atlantic
VM28-122
Indo-Pacific
LGM
late HOL

Fig. 5.

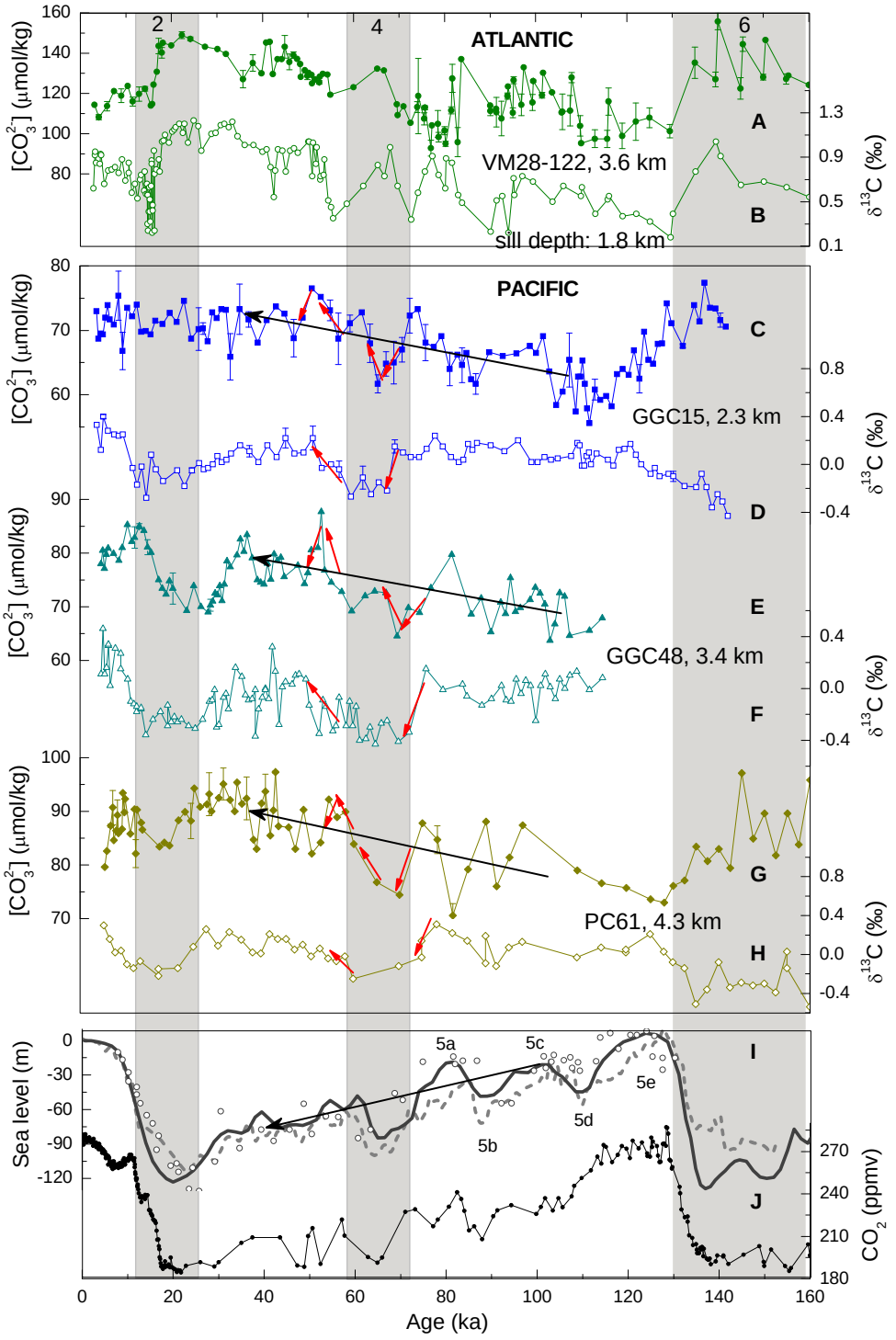
ATLANTIC
VM28-122, 3.6 km
Sill depth: 1.8 km
PACIFIC
GGC15, 2.3 km
GGC48, 3.4 km
PC61, 4.3 km
2
4
6
5a
5b
5c
5d
5e
A
B
C
D
E
F
G
H
I
J
[CO3 2-] (µmol/kg)
δ13C (‰)
Sea level (m)
CO2 (ppmv)
Age (ka)

Fig. 6.

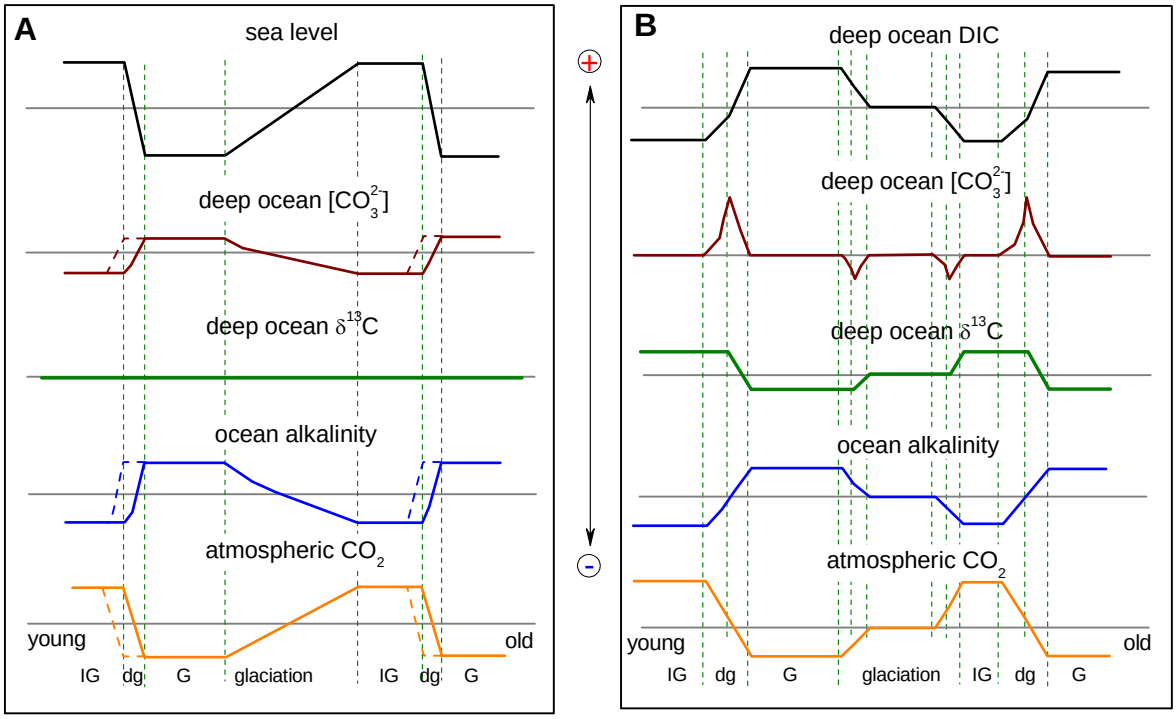
A
sea level
deep ocean [CO3 2-]
deep ocean δ13C
ocean alkalinity
atmospheric CO2
young
old
IG
dg
G
glaciation
IG
dg
G
+
-
B
deep ocean DIC
deep ocean [CO3 2-]
deep ocean δ13C
ocean alkalinity
atmospheric CO2
young
old
IG
dg
G
glaciation
IG
dg
G

Fig. 7.

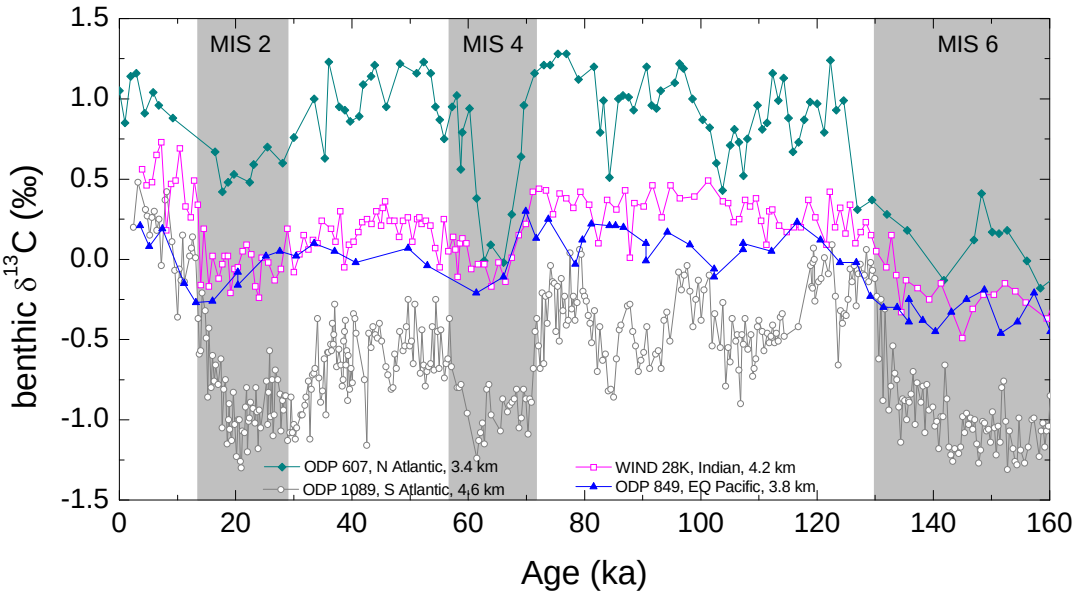
MIS 2
MIS 4
MIS 6
benthic δ13C (‰)
Age (ka)
ODP 607, N Atlantic, 3.4 km
ODP 1089, S Atlantic, 4.6 km
WIND 28K, Indian, 4.2 km
ODP 849, EQ Pacific, 3.8 km

Fig. 8.

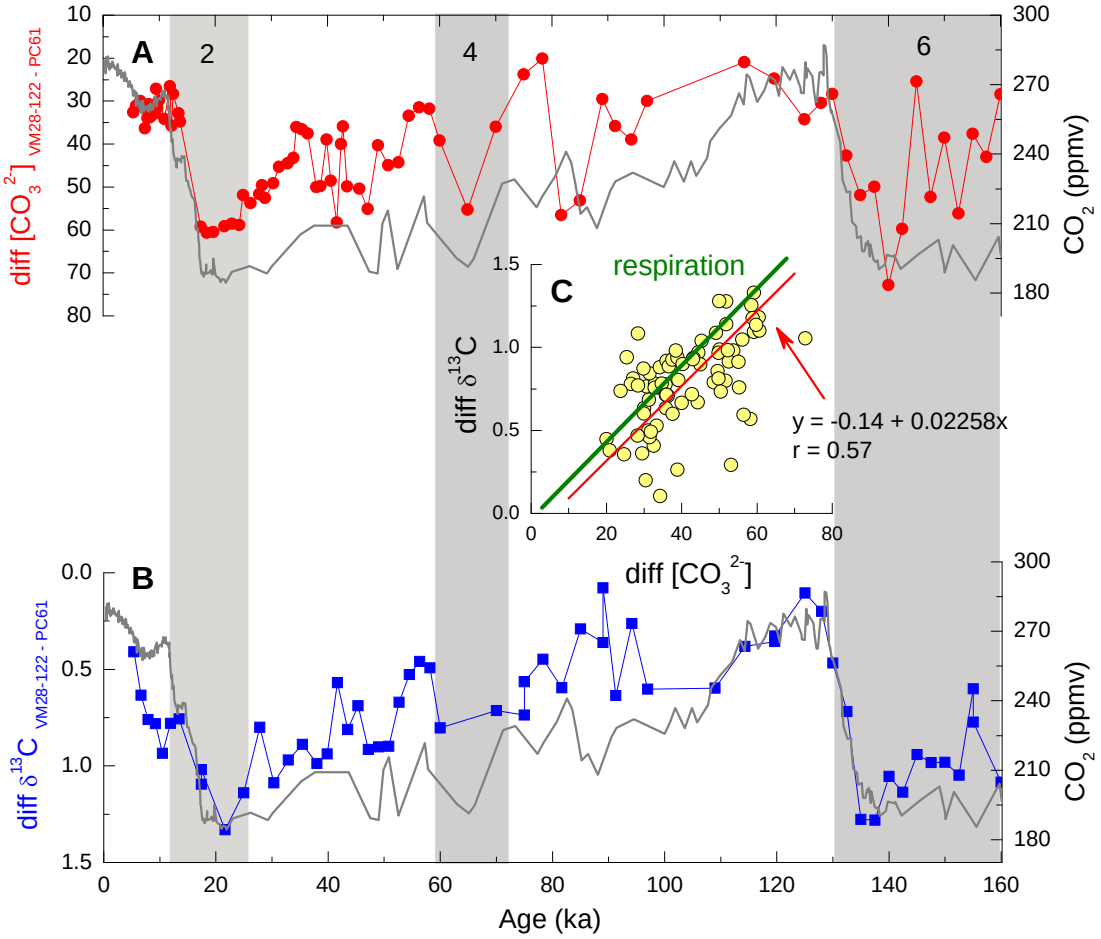
A
2
4
6
diff [CO3 2-] VM28-122 - PC61
CO2 (ppmv)
C
respiration
diff δ13C
y = -0.14 + 0.02258x
r = 0.57
B
diff [CO3 2-]
diff δ13C VM28-122 - PC61
CO2 (ppmv)
Age (ka)

Fig. 9.

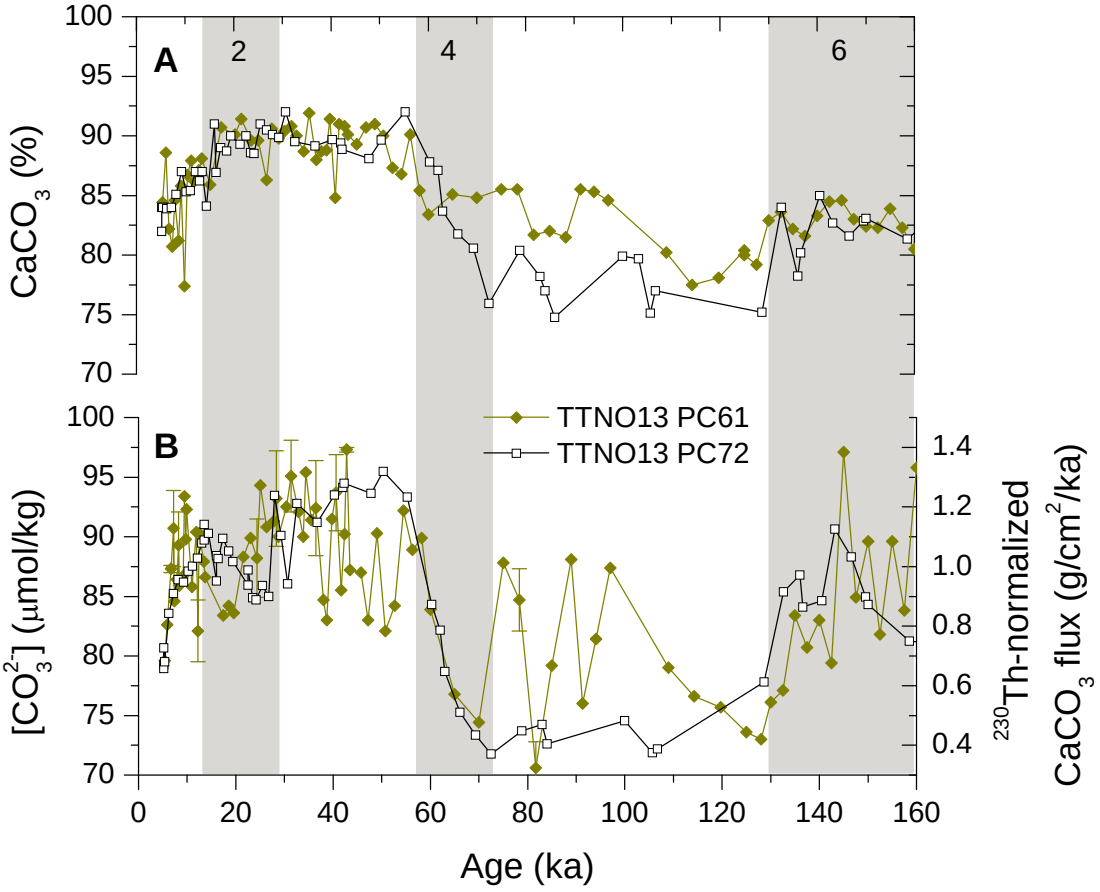
A
B
2
4
6
TTNO13 PC61
TTNO13 PC72
CaCO3 (%)
[CO3 2-] (µmol/kg)
230Th-normalized CaCO3 flux (g/cm2/ka)
Age (ka)

Fig. 10.

Supplementary figures

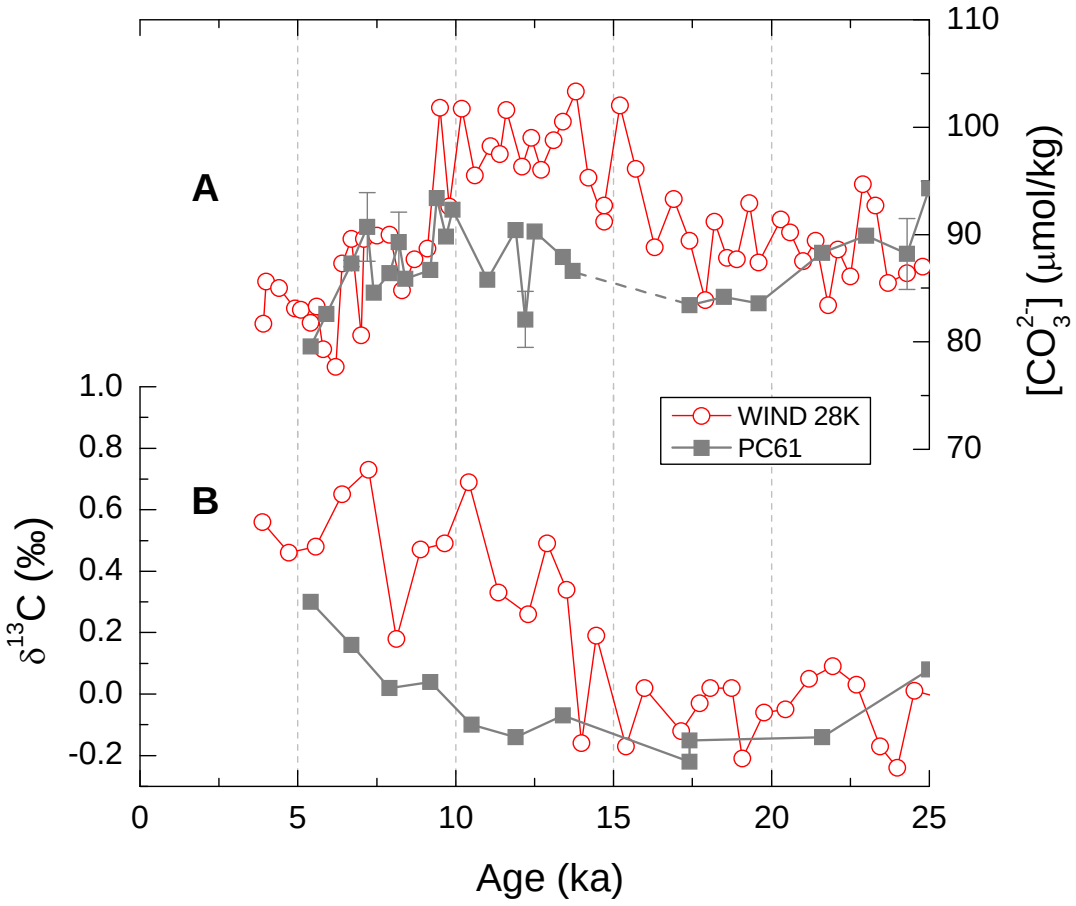

Fig. S1. Comparison of deep water [CO_3^{2-}] (**A**) and $\delta^{13}C$ (**B**) in cores PC61 (0.86°S, 140°W, 4276 m) (this study) from the equatorial Pacific Ocean and WIND 28K (10.2°S, 51.8°E, 4147 m) (Yu et al., 2010) from the Indian Ocean during the last 25 ka. Both [CO_3^{2-}] records show spikes during the last deglaciation, but [CO_3^{2-}] at PC61 peaked at a later age (~9 ka) than [CO_3^{2-}] at WIND 28K (~14-10 ka). This age offset is probably an artifact of strong bioturbation due to low sedimentation rates at site PC61 (Fig. 2D), highlighting the need for high-resolution in the Pacific Ocean.

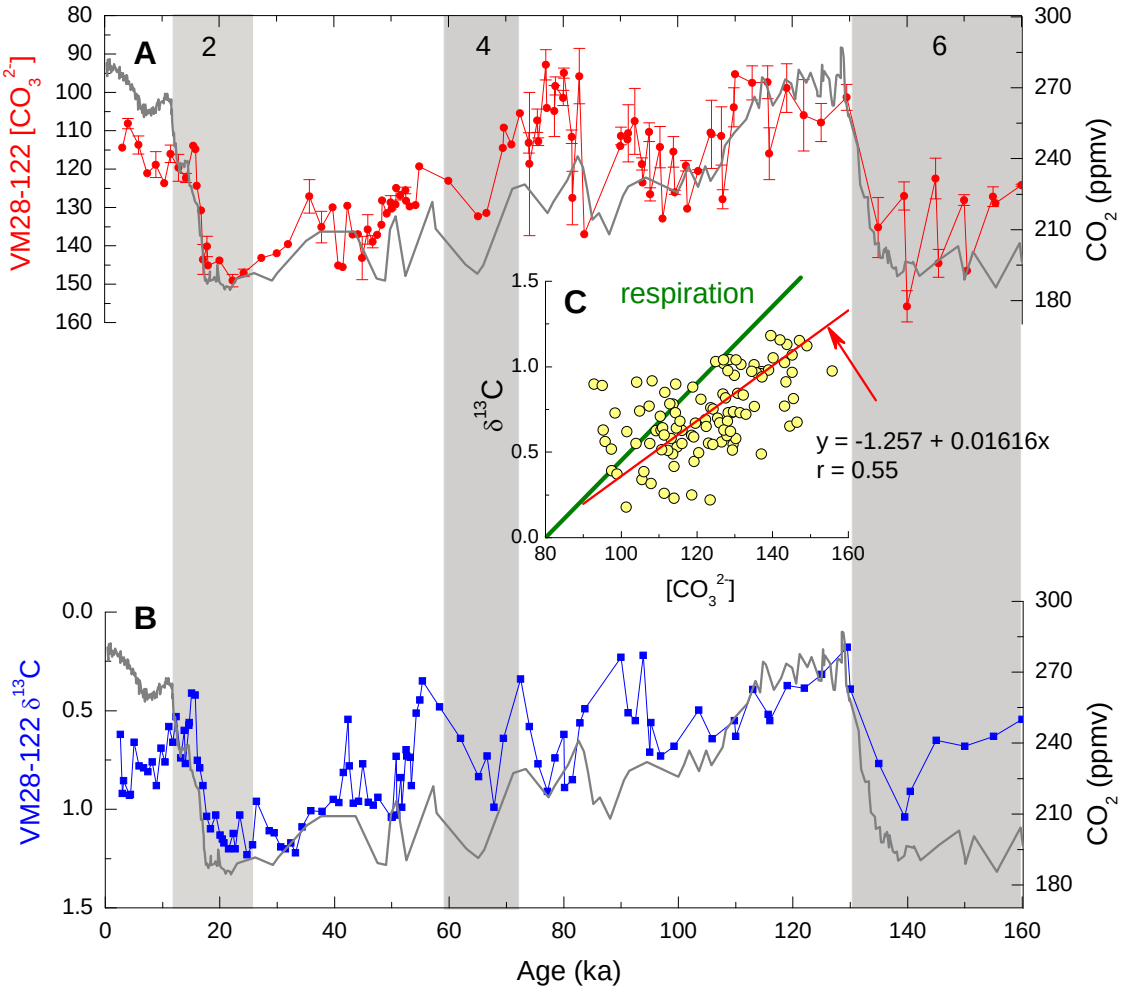

Fig. S2. Variations of deep water $[CO_3^{2-}]$ (**A**) and $\delta^{13}C$ (**B**) in core VM28-122 during the last 160 ka. Both $[CO_3^{2-}]$ and $\delta^{13}C$ correlated with atmospheric CO_2 (Lüthi et al., 2008), but they plot along a different trend from the Redfield slope on the $\delta^{13}C$-$[CO_3^{2-}]$ space (Yu et al., 2008) (**C**).

References:

Lüthi, D., Floch, M.L., Bereiter, B., Blunier, T., Barnola, J.M., Siegenthaler, U., Raynaud, D., Jouzel, J., Fischer, H., Kawamura, K., Stocker, T.F., 2008. High-resolution carbon dioxide concentration record 650,000–800,000 years before present. Nature 453, doi:10.1038/nature06949.

Yu, J., Broecker, W., Elderfield, H., Jin, Z.D., McManus, J., Zhang, F., 2010. Loss of carbon from the deep sea since the Last Glacial Maximum. Science 330, 1084-1087, doi: 1010.1126/science.1193221.

Yu, J.M., Elderfield, H., Piotrowski, A., 2008. Seawater carbonate ion-$\delta^{13}C$ systematics and application to glacial-interglacial North Atlantic ocean circulation. Earth Planet. Sci. Lett. 271, 209-220. doi:210.1016/j.epsl.2008.1004.1010.